Virginia Polytechnic Institute
and State University
Chemistry Department
Blacksburg, Virginia 24061

FINAL TECHNICAL REPORT

A FUNDAMENTAL APPROACH TO ADHESION: SYNTHESIS, SURFACE ANALYSIS, THERMODYNAMICS AND MECHANICS

by

Betty Beck, Ranjani Siriwardane and James P. Wightman

Prepared for

National Aeronautics and Space Administration

April, 1981

Grant NSG-1124

NASA-Langley Research Center
Hampton, Virginia 23665
Materials Division
Donald J. Progar

Department of Chemistry
Virginia Polytechnic Institute and State University
Blacksburg, Virginia 24061

FOREWARD

This final technical report summarizes our research on a fundamental study of adhesion. The results of the past year's efforts at Virginia Polytechnic Institute and State University are described starting on p. iii.

A second major thrust of this year's effort was polymer synthesis carried out by Paul M. Hergenrother, Adjunct Research Professor, at NASA-LaRC. A summary of this work on polymer synthesis is given in Appendix III.

Copies of the surface analysis activities published during the total grant period (1974-1981) are contained in Appendix IV.

TABLE OF CONTENTS

LIST OF TABLES

LIST OF FIGURES

GLOSSARY

TECHNIQUES

EDAX - Energy dispersive analysis of x-rays

ESCA - Electron spectroscopy for chemical analysis

SEM - Scanning electron microscopy

CHEMICALS

DMF - Dimethylformamide

(ME)PPQ - (Monoether) Polyphenylquinoxaline

OTHERS

AF - Atomic fraction

AMR - Advanced Metals Research

BE - Binding energy

BET - Brunauer, Emmett and Teller

CAA - Chromic acid anodized

i.e.p. - Isoelectric point

LSS - Lap shear strength

PAA - Phosphoric acid anodized

RAE - Royal Air Force Establishment

LaRC - Langley Research Center

I. INTRODUCTION

During the current grant period, our experimental program has focused on

(i) the characterization of pretreated and primed Ti 6-4 surfaces by SEM/EDAX (scanning electron microscopy/energy dispersive analysis of X-rays) and ESCA (electron spectroscopy for chemical analysis),

(ii) the characterization of fractured lap shear bonded Ti 6-4 specimens by SEM/EDAX and ESCA, and

(iii) the characterization of TiO_2 powders by a number of surface techniques

The scope of the program is outlined in Table I.

The rationale for the study of TiO_2 powders is given below. Titanium and its alloys show superior corrosion resistance due to protection by an inherent oxide film at low and moderate temperatures (1). The nature of this oxide film has been the subject of a number of papers (2-9). The role of this oxide film in determining bond strength and bond durability is not yet established as judged by the contradictory evidence in a number of recent papers (2-4, 6-11). The particular crystal phase of TiO_2 making up the oxide layer on a Ti 6-4 surface has not been established unambiguously.

There are only a limited number of studies which report the properties of this surface oxide layer measured in situ. Indeed, a number of significant surface properties of the oxide layer cannot be measured readily on a flat coupon. These surface properties include surface area, surface charge and the enthalpy change on spreading a primer solution across the

TABLE I

SCOPE OF EXPERIMENTAL PROGRAM

SAMPLE	TECHNIQUE	INFORMATION
Pretreated Ti 6-4	SEM	Surface Morphology
	ESCA	Surface Composition
Primed Ti 6-4	SEM	Surface Morphology
	ESCA	Surface Composition
Fractured LSS(Ti 6-4)	SEM	Surface Morphology
	ESCA	Surface Composition
TiO_2 Powders	SEM	Surface Morphology
	ESCA	Surface Composition
	Immersional Calorimetry	Heats of Immersion
	X-ray Diffraction	Crystal Structure
	Microelectrophoresis	Surface Charge
	Nitrogen Adsorption	Surface Area
	Water Adsorption	Hydrophilicity

Ti 6-4 adherend. Thus a study was initiated to characterize the surface properties of both anatase and rutile TiO_2.

II. EXPERIMENTAL

A. Materials

1. Ti 6-4 Coupons - Fifty-six (56) pretreated and primed Ti 6-4 coupons were supplied by personnel at the Boeing Company under NASA Contract NAS1-15505. The chemical pretreatments and primers used are listed in Table II. Details of the various chemical pretreatments are contained in Appendix I.
2. Adhesive Systems - Ten (10) adhesive systems were used in the bonding of the pretreated and primed Ti 6-4 adherends by the Boeing Co. under NASA Contract NAS1-15605. The adhesive systems studied in the present work are listed in Table III. Details of the adhesive resins are given in Appendix II.
3. Fractured Lap Shear Samples - These samples were supplied by personnel at the Boeing Company under NASA Contract NAS1-15605. A total of 150 samples were supplied resulting from the combination of 8 chemical pretreatments and 10 adhesive systems at 2 test temperatures. The particular samples which were characterized in the current grant period are listed in Table IV. The average lap shear strength is listed and also the strength of the particular sample used in our study is given in parenthesis.
4. Titania Powders - The four titania powders characterized in this study are listed in Table V. The crystal structure was determined by X-ray diffraction.
5. LaRC-13 and PPQ Polymers - These polymers were obtained from personnel at NASA-LaRC.

TABLE II

LISTING OF CHEMICAL PRETREATMENTS AND PRIMERS
USED ON Ti 6-4 ADHERENDS

Pretreatment	Primer
Chromic Acid Anodize	NR150A2
Phosphoric Acid Anodize	NR150A2 + 30% Al
Pasa-Jell 107	NR150B2
Phosphate-Fluoride (Boeing)	NR150B2 + 30% Al
Phosphate-Fluoride (Picatinny)	PPQ
Phosphate-Fluoride (Grit Blast)	LARC-13 + 30% Al
Turco	BR-34
RAE	

TABLE III

LISTING OF ADHESIVE SYSTEMS

Boeing Designation	Composition
L13	NASA LARC-13 Polyimide + 30 wt % Al powder
L13M1	NASA LARC-13 Polyimide + Amoco-amide-imide AI-1130 + Al powder
L13M2	Methyl nadic capped polymer + 20 mole % m-phenylene diamine
PPQ	Monoether Polyphenylquinoxaline
PPQM1	Monoether Polyphenylquinoxaline + boron powder

TABLE IV

LISTING OF LAP SHEAR SAMPLES

Boeing Designation*	Lap Shear Strength in psi
PPQ-A-7, RT	5250(4650)
PPQ-A-2, 450°	2280(2820)
PPQ-D-5, RT	2240(1950)
PPQ-D-4, 450°	2420(3000)
PPQ M1-A-7, RT	2320 (2290)
PPQ M1-A-4, 450°	1030(972)
PPQ M1-D-5, RT	930(720)
PPQ M1-D-8, 450°	1000(1010)
L13-A-2, RT	2980(2170)
L13-A-2, 450°	2200(2168)
L13-D-5, RT	1650(870)
L13-D-6, 450°	1490(0)
L13 M1-A-9, RT	2630(2750)
L13 M1-A-6, 450°	1910(1940)
L13 M1-D-9, RT	1330(1260)
L13 M1-D-6, 450°	1130(808)
L13 M2-A-2, 450°	540(410)
L13 M2-D-8, 450°	400(440)

*Adhesive resin (PPQ or L13) - chromic acid anodize (A) or phosphate-fluoride (D) - sample no. - test temperature.

TABLE V

LISTING OF TITANIA (TiO_2) POWDERS

Powder	Crystal Structure	Surface Area(m^2/g)	Supplier
A1	Anatase	10.5	Glidden
A2	Anatase (87%)	11.0	Cabot
	Rutile (13%)		
R1	Rutile	7.04	Glidden
R2	Rutile	7.82	duPont

B. Methods and Procedures

1. Electron Spectroscopy for Chemical Analysis (ESCA) - ESCA data were collected on a DuPont 650 photoelectron spectrometer with a magnesium anode ($K\alpha_{1,2}$ = 1253.6 ev) and direct display of the spectra on an x-y recorder. The carbon 1s level (taken at 285.0 ev) was used to evaluate the work function of the spectrometer. Circular (6.4 mm diameter) samples were mounted on the copper sample probes using double sided adhesive tape.

2. Scanning Electron Microscopy/Energy Dispersive Analysis of X-rays (SEM/EDAX) - SEM photomicrographs at various magnifications were obtained on an AMR scanning electron microscope (Advanced Metals Research Corporation Model 900). Approximate vertical dimensions of each photomicrograph appear at the right in the figures, and the corresponding magnification is listed in each caption. Most SEM samples were run after ESCA analysis. A thin ($\sim$ 20 nm) film of Au-Pd Alloy was vacuum-evaporated onto the samples to enhance conductivity of insulating samples which were mounted on an Al sample stub with copper conductive tape. A rapid semi-quantitative elemental analysis was obtained on selected samples with an EDAX International Model 707A energy-dispersive X-ray fluorescence analyzer attached to the AMR-900 SEM. A photographic record of each EDAX spectrum was made using a camera specially adapted for the EDAX oscilloscope.

3. Surface Areas - The surface areas of the titania powders were measured by the BET method (12) using nitrogen adsorption at -196°C. Matheson ultra high purity (99%) nitrogen was used as the adsorbate in the surface area studies. A Micromeritics Model 2100 D Surface Area-Pore Volume Analyzer was used. The powders were outgassed for 1 hour at $< 1 \times 10^{-4}$ torr at 100°C prior to the surface area measurements.

4. X-ray Diffraction - The crystal structures of the titania powders were measured on a Diano-XRD Model 8000 diffractometer using Cu Kα radiation.

5. Immersional Calorimetry - Heats of wetting of the titania powders in various liquids were measured in a Calvet MS 70 Microcalorimeter at 36°C. The powders were outgassed for 2 hr under vacuum (< $1x10^{-4}$ torr) over a temperature range (25° - 400°C) prior to the heat of wetting measurement. 5% PPQ polymer solution was prepared by dissolving the polymer in 1:1 xylene : m-cresol solution. 22% by weight LARC-13 was dissolved in dimethyl formamide (DMF). Heats of immersion of the powder in two solvents xylene : m-cresol and DMF were first determined. Heats of immersion of all four powders in 5% PPQ and 22% LARC-13 and of anatase in 1%, 3% PPQ solutions were also determined.

6. Microelectrophoresis - The electrophoretic mobility (u) and isoelectric point (i.e.p.) of the titania powders were determined using a Rank Mark II microelectrophoresis apparatus.

Analytical grade potassium nitrate was used to prepare 0.02 M solutions, whose pH was varied by appropriate addition of either nitric acid or potassium hydroxide for use in the electrophoretic measurements (13). For comparison purposes, pH was also adjusted using HCl and NaOH. Powders were dispersed ultrasonically in the potassium nitrate solutions and transferred to the microelectrophoresis cell which was constructed from silica. The cell was mounted in a perspex thermostatted tank (25°C) attached to the stage of a microscope. The particles were observed by dark field illumination and about five particles were timed at each stationary level in both directions.

7. Water Adsorption - Water adsorption on the titania powders was measured using a differential capacitance manometer [Baratron MS 100 cell] in a constant volume system constructed with Teflon stopcocks. The powders were outgassed at < 1×10^{-4} torr for 2 hrs over a temperature range (25°-400°C) prior to the adsorption measurements. The quantity of water adsorbed

was calculated assuming ideal gas behavior. Readsorption isotherms were determined after heating the equilibrated samples at the specified temperature for 2 hours.

8. Surface Acidity - Indicator solutions of p-nitro phenol (Fisher)/ toluene, alizarin (Fisher)/toluene and o-nitro phenol (Eastman)/iso octane were used for acidity measurements. Indicator solutions were prepared by dissolving 1 mg of the indicator in 25 cc of solvent. Color changes of the adsorbed indicators were observed by mixing 1 g of the powder with 2 ml of the indicator. The color changes were also observed on the samples evacuated at 300°C for 2 hrs, in glass ampoules with break off tips.

III. RESULTS AND DISCUSSION

A. Pretreated Ti 6-4 Surfaces

Representative SEM photomicrographs of the chemically pretreated Ti 6-4 adherends are shown in Figures 1-3. A representative SEM photomicrograph of a chromic acid anodized Ti 6-4 adherend is shown in Figure 1 A. In the substrate, there appears to be a surface layer containing minute cracks or fissures of irregular shape. At the highest (10,000X) magnification (not shown), the whole surface layer appears to be sponge-like presumably due to the presence of small diameter pores not resolved in the SEM. A representative SEM photomicrograph of a phosphoric acid anodized Ti 6-4 adherend is shown in Figure 1 B. The surface features here are similar to those described for the chromic acid anodized cases.

A representative SEM photomicrograph of a phosphate-fluoride [Boeing] treated Ti 6-4 adherend is shown in Figure 2 A. Fairly well defined alpha (gray) and beta (white) phases appear as surface features in contrast to their absence on both anodized surfaces. At higher (10,000A) magnification (not shown), the beta phase crystals are poorly defined but the alpha phase

Figure 1.

SEM photomicrographs (2,000x) of
(A) chromic acid anodized and
(B) phosphoric acid anodized
Ti 6-4 adherends.

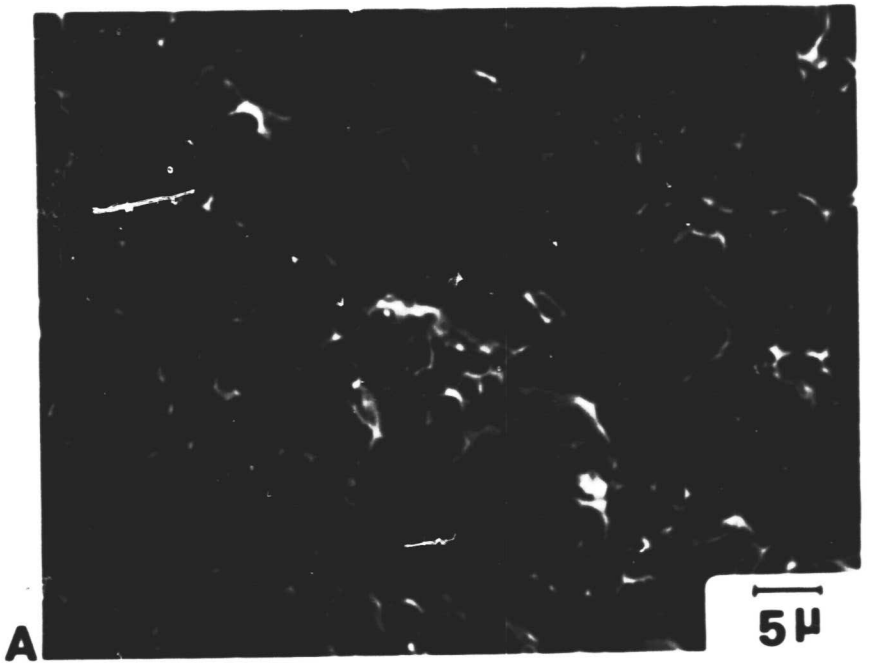
A
5μ

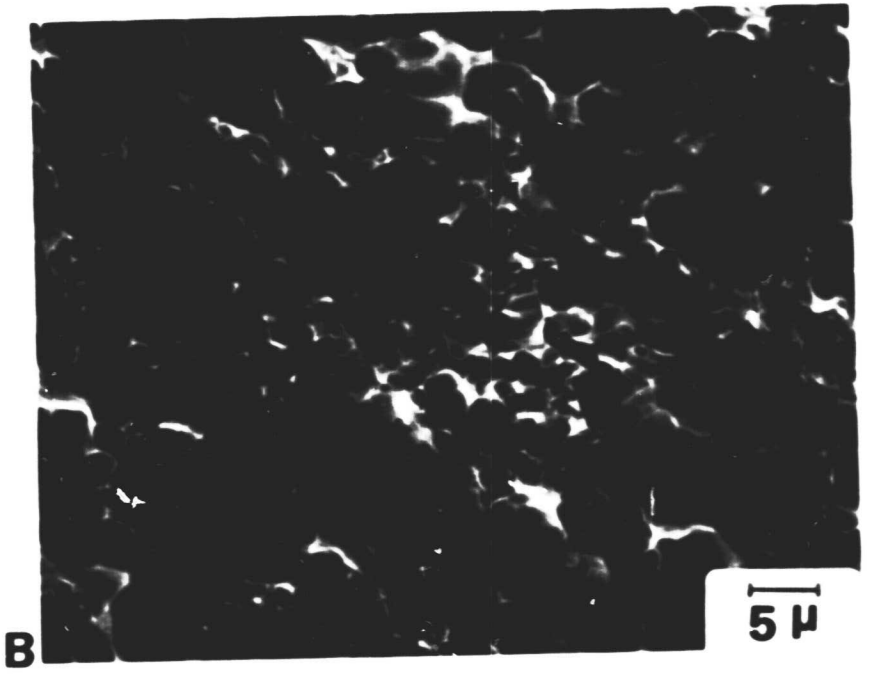
B
5μ

Figure 2.

SEM photomicrographs (2,000x) of (A) phosphate-fluoride [Boeing], (B) phosphate-fluoride [Picatinny], (C) phosphate-fluoride [grit blast], and (D) Pasa-Jell treated Ti 6-4 adherends.

Figure 2. SEM photomicrographs (2,000X) of (A) phosphate-fluoride [Boeing], (B) phosphate-fluoride [Picatinny], (C) phosphate-fluoride [grit blast], and (D) Pasa-Jell treated Ti 6-4 adherends.

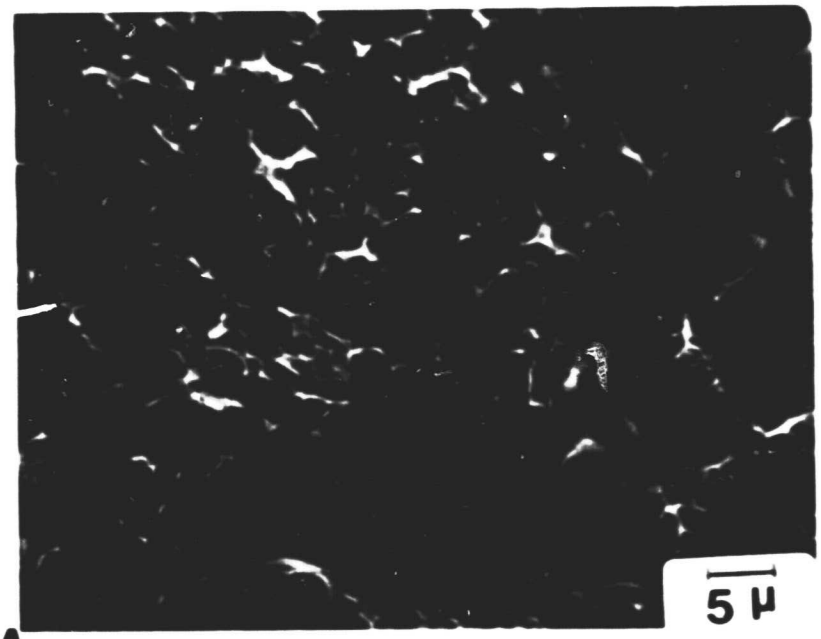

A

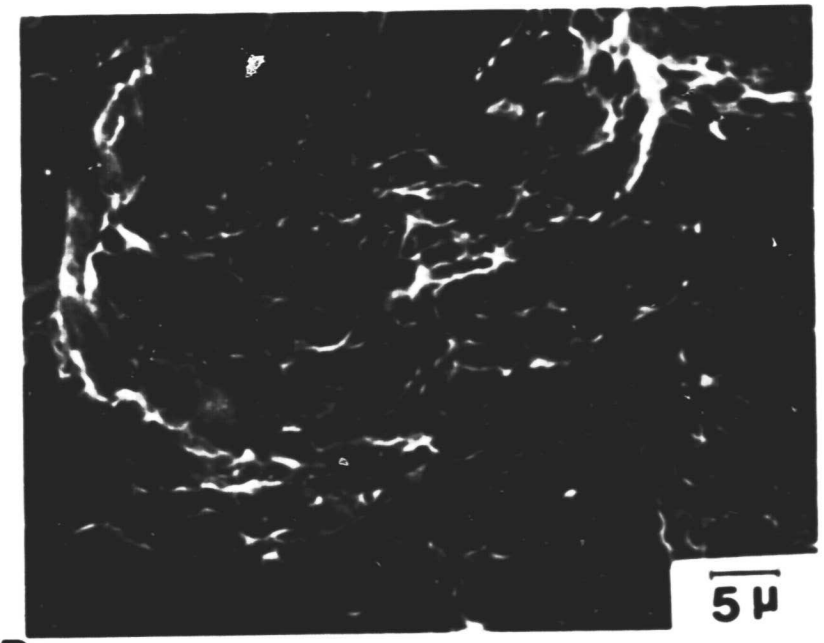

B

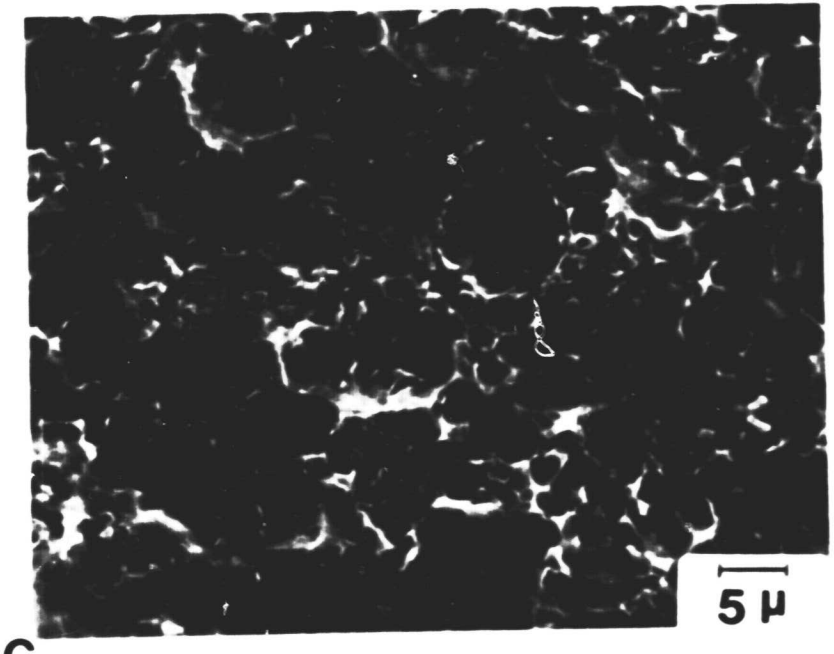

C

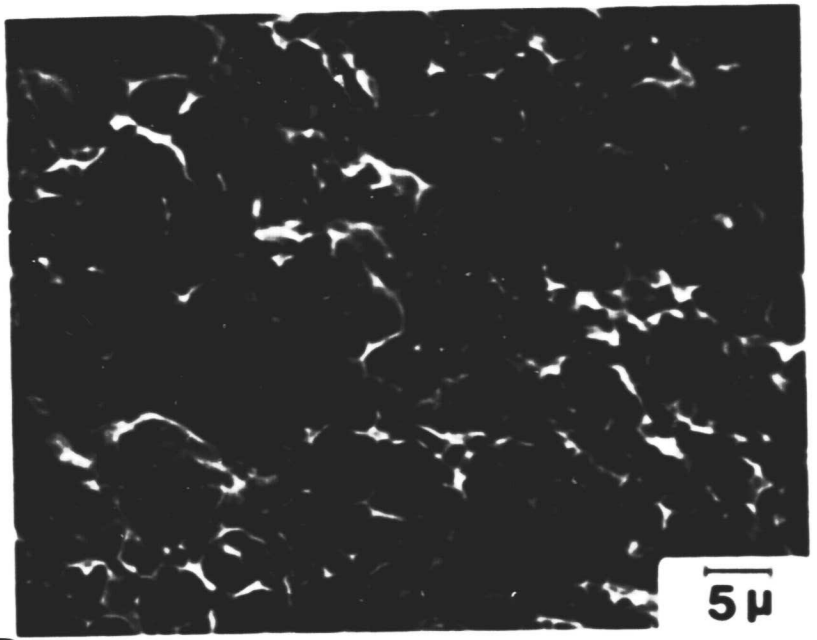

D

Figure 3.

SEM photomicrographs (2,000x) of (A) Turco and (B) RAE [$NaOH/H_2O_2$] treated Ti 6-4 adherends.

Figure 3. SEM photomicrographs (2,000X) of (A) Turco and (B) RAE [$NaOH/H_2O_2$] treated Ti 6-4 adherends.

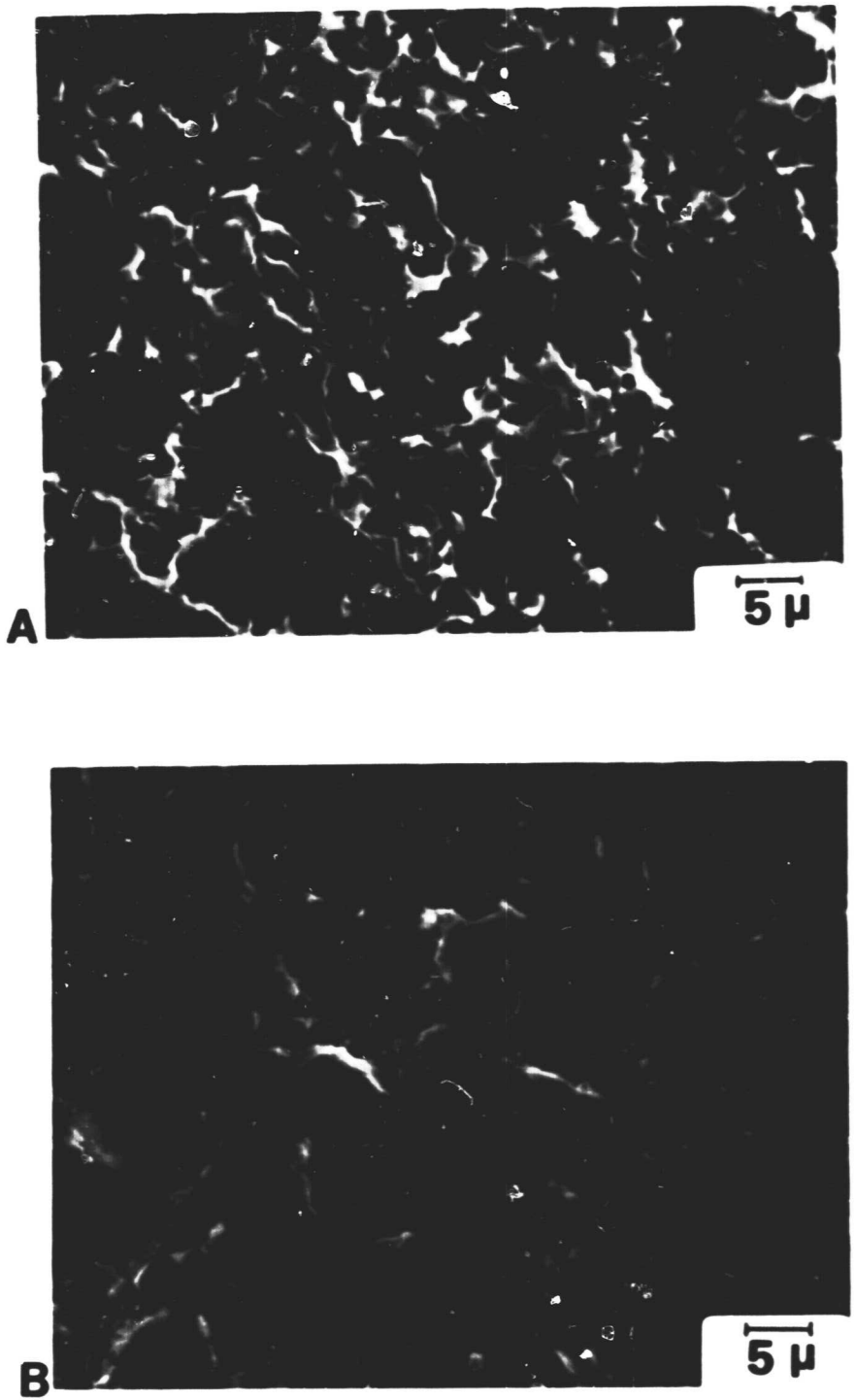
A
5 µ
B
5 µ

shows regularly spaced edges about 100 nm apart. Representative SEM photomicrographs of phosphate-fluoride [Picatinny] and of phosphate-fluoride [grit blast] treated Ti 6-4 adherends are shown in Figures 2 B and 2 C, respectively. The surface morphology is similar for all three of these phosphate-fluoride treated surfaces. A representative SEM photomicrograph of the Pasa-Jell treated Ti 6-4 adherend is shown in Figure 2 D. The surface features are similar to those observed for the phosphate-fluoride treatment. Closer inspection of Figure 2 D or of photomicrographs obtained at higher magnification show that the surface is littered with "popcorn" particles whose identity was not established. The conclusion here is that the four acidic etches give rise to a similar surface morphology for Ti 6-4 adherends.

A representative SEM photomicrograph of a Turco treated Ti 6-4 adherend is shown in Figure 3 A. The surface features for this alkaline etch are in sharp contrast to those following the acidic pretreatments. The beta phase appears to have grown at the expense of the alpha phase and exists as highly fragmented structures. A representative SEM photomicrograph of RAE alkaline hydrogen peroxide treated Ti 6-4 is shown in Figure 3 B. The surface features here are unlike any of the preceding ones. A mottled surface is obtained having no distinct features.

In summary, both the anodized surfaces have similar surface features as is the case for the four acid etched surfaces. By contrast, there are no similarities in the SEM photomicrographs of the alkaline treated surfaces.

The ESCA results for the different pretreated Ti 6-4 adherends are given in Table VI. The binding energy (BE) in ev of each photopeak and the atomic fraction (AF) for each element calculated using equation [1] are tabulated.

$$AF_i = \frac{A_i/\sigma_i}{\Sigma\, A_i/\sigma_i} \qquad [1]$$

TABLE VI

ESCA ANALYSIS OF Ti 6-4 SURFACES AFTER CHEMICAL PRETREATMENT

	Chromic Acid Anodize		Phosphoric Acid Anodize		Pasa-Jell		Phosphate-Fluoride [P]		Turco[14]		RAE	
Photopeak	BE	AF	BE	AF	BE	AF	BE	AF	BE	AF	BE	AF
Na 1s									1071.6	0.06		
F 1s	688.6 685.4	0.03	685.4	0.02	685.2	0.01	684.8	0.01				
Cr $2p_{3/2}$					578.0	0.01						
O 1s	530.4	0.19	530.6	0.24	530.8	0.44	530.2	0.29	530.9	0.20	530.4	0.48
Ti $2p_{3/2}$	458.8	0.08	459.2	0.10	458.8	0.15	458.6	0.10	458.6	0.09	459.0	0.18
N 1s	400.2	0.03	400.4	0.01	400.4	0.01	400.0	0.02	400.5	0.01	400.4	0.01
Ca $2p_{3/2}$					347.8	0.01	349.0	0.02			347.4	0.04
C 1s	(285.0)	0.67	(285.0)	0.60	(285.0)	0.38	(285.0)	0.53	(285.0)	0.64	(285.0)	0.26
P $2p_{3/2}$			134.0	0.02			133.4	0.02				
Al 2s											119.2	0.03

A_i is the area of the i-th photoelectron peak and σ_i is the photoelectron cross-section (15).

In addition to the photopeaks for ubiquitous carbon and for titanium and oxygen, significant quantities of nitrogen and fluorine were detected on the chromic acid anodized Ti 6-4. The binding energy of nitrogen suggests the presence of a nitride. It is worthwhile to note that the same nitrogen photopeak was observed on the Ti 6-4 surface following all six pretreatments. The fluorine peak appeared as a doublet with the higher binding energy peak at 687.6 ev being the larger. This result suggests two different bonding states of fluorine in the surface. The ESCA results in Table VI for both of the anodized surfaces are similar except that a small phosphorus photopeak is observed and the fluorine photopeak appears as a singlet for the phosphoric acid anodized Ti 6-4.

The ESCA results in Table VI for the phosphate-fluoride [Picatinny] treated Ti 6-4 indicate the presence of trace calcium and phosphorus on the surface. The ESCA results in Table VI for both of the acid etched surfaces are similar except a chromium photopeak is observed for the Pasa-Jell etch instead of a phosphorus photopeak.

The ESCA results in Table VI indicate the absence of fluorine for both alkaline etched surfaces. A significant quantity of sodium is noted on the Turco treated Ti 6-4 surface. Trace quantities of aluminum and calcium are noted on the Ti 6-4 adherend surface after treatment by the RAE process.

B. Primed Ti 6-4 Surfaces

SEM photomicrographs of the PPQ-CAA and LaRC-PAA primed Ti 6-4 adherends are shown in Figure 4. The PPQ primed surface shows two morphologies. Opaque and transparent regions of the primed surfaces were noted on visual examination. The photomicrograph in Fig. 4A was taken of an opaque region. The morphology

Figure 4.

SEM photomicrographs of (A) PPQ primed Ti 6-4 [opaque region] (1,600X), (B) PPQ primed Ti 6-4 [transparent region] (900X), and (C) LaRC 13 primed Ti 6-4(800X).

Figure 4. SEM photomicrographs of (A) PPQ primed Ti 6-4 [opaque region] (1,600X), (B) PPQ primed Ti 6-4 [transparent region] (900X), and (C) LaRC 13 primed Ti 6-4(800X).

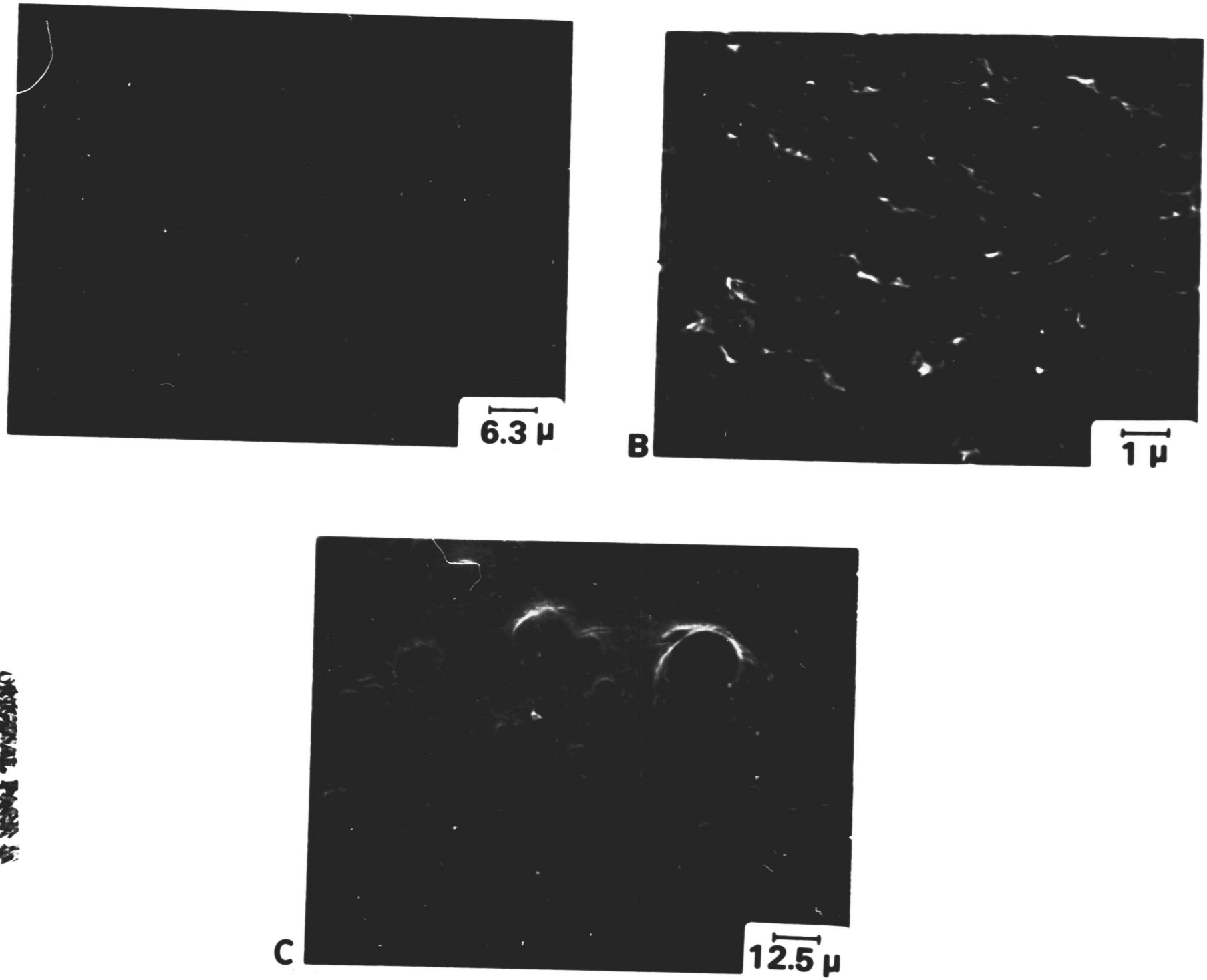

seen in Fig. 4A may be due to crystallized PPQ. A similar morphology has been observed by Desai and Wilkes for the solvent induced crystallization of polyethylene terephthalate (16). The photomicrograph in Fig. 4B was taken of a transparent region. The chromic acid anodized Ti 6-4 substrate is visible through amorphous primer film. The Al filler is apparent in the SEM photomicrograph of the LaRC 13 primer shown in Fig. 4C. The Ti 6-4 substrate is not visible in this case. The mosaic appearance may arise from thermal retraction during cooling after primer curing at elevated temperature. No Ti signal was observed in the EDAX spectra of any of these primed adherends.

The ESCA results for the primed surfaces are shown in Table VII. Average values for two separate LaRC-13 primed surfaces (CAA and PAA) are shown. Again, no Ti signal was observed indicative of a thick primer coat. Thus, the ESCA spectra observed for the primed adherend is just that of the primer itself. The fact that no Al signal was observed suggests complete coating of these filler particles by primer film. The C 1s region shows a unique ESCA fingerprint for LaRC-13 including a shake-up satellite at 291.5 eV and a > C=O peak at 288.5 ev..

The ESCA results for PPQ are the average values for four separate primed surfaces. The primed surfaces were (1) CAA-opaque region; (2) CAA-transparent region; (3) PAA and (4) thin film deposited from a m-cresol/xylene solution. There were no significant differences in either the binding energy or atomic fraction values for the four primed surfaces. Again, the ESCA spectra observed is that of PPQ itself and is not dependent on the substrate. There were no significant differences in the ESCA spectra of the opaque and transparent regions of the primer on CAA Ti 6-4 in contrast to the SEM photomicrographs.

TABLE VII

ESCA RESULTS FOR PRIMED Ti 6-4 ADHERENDS

Primer	Photopeak	B.E.(ev)	A.F.
LaRC-13	O 1s	532.3 ± 0.01	0.16 ± 0.02
	N 1s	400.5 ± 0.1	0.050 ± 0.006
	C 1s	285.0,288.5,291.5	0.80 ± 0.02
PPQ	O 1s	533.5 ± 0.2	0.048 ± 0.010
	N 1s	399.2 ± 0.1	0.062 ± 0.008
	C 1s	285.0,291.5	0.89 ± 0.01

C. Fractured Lap Shear Samples - PPQ

The fractured lap shear samples are discussed by polymer type, pretreatment and strength test temperature. An extensive series of SEM photomicrographs were taken of the numerous samples studied in the present work. It is not the purpose of this report to present and discuss all of these SEM photomicrographs. Rather, the approach has been to point out similarities to what has already been presented. A great deal of material has thus been eliminated without sacrificing an understanding of the results.

1. Polyphenylquinoxaline - chromic acid anodize-room temperature [PPQ-A-7, RT] - Both members of all the fractured lap shear test samples were photographed using a Canon 35 mm camera with a macro lens. The 35 mm photograph of the above sample is shown in Figure 5 A. A cohesive failure mode is assigned as judged by the fact that no adherend surface is observed on either member. A circular 6.3 mm (0.25 inch) diameter sample was punched out of one of the members. This circular sample was photographed with a Bausch and Lomb Stereo Microscope. The optical photomicrograph of the above sample is shown in Figure 5 B. Again, only scrim cloth is visible indicative of cohesive failure. SEM photomicrographs of this circular sample are shown in Figures 5 C and 5 D. The fibers appear dewetted (Fig. 5 C) but their orientation is not disrupted. Primarily brittle failure has occurred with some plastic deformation as seen by the plastic flow lines on the right side of Fig. 5 D.

The ESCA results are listed in Table VIII. The presence of the glass scrim cloth is evidenced by the Si 2p photopeak at 103.6 ev. This value is in good agreement with the value of 103.3 ev reported by Kang (17) for α-quartz. The N 1s photopeak is characteristic of polyphenylquinoxaline as described in Table VII. The O 1s photopeak appears at a higher binding

Figure 5.

Photomicrographs of [PPQ-A-7, RT]
(A) original lap shear specimen (3X),
(B) punched SEM/ESCA sample (14X),
(C) SFM/fracture surface (95X), and
(D) SEM/fracture surface (475X).

Figure 5. Photomicrographs of [PPQ-A-7, RT] (A) original lap shear specimen (3X), (B) punched SEM/ESCA sample (14X), (C) SEM/fracture surface (95X), and (D) SEM/fracture surface (475X).

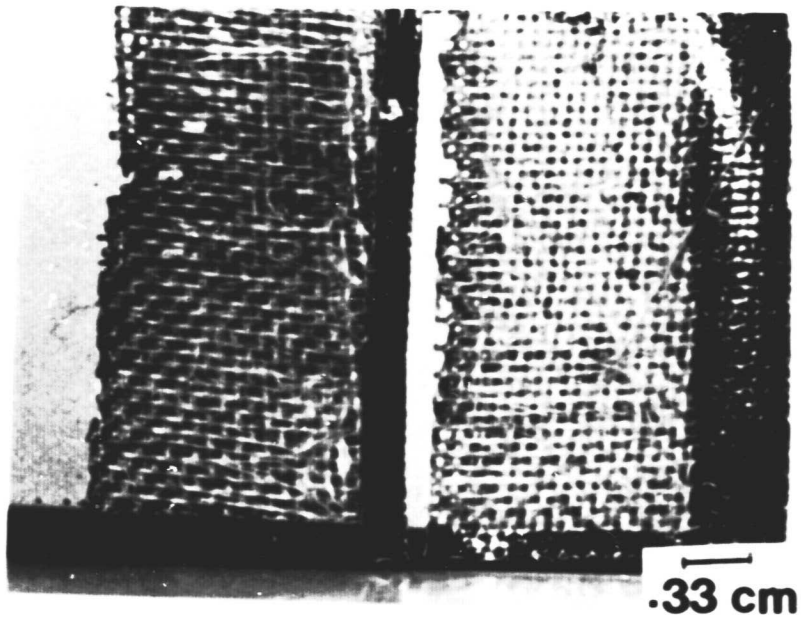

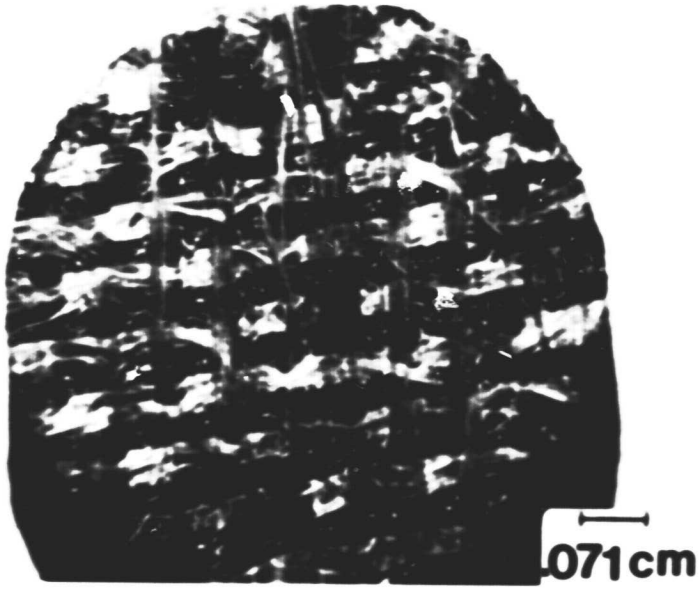

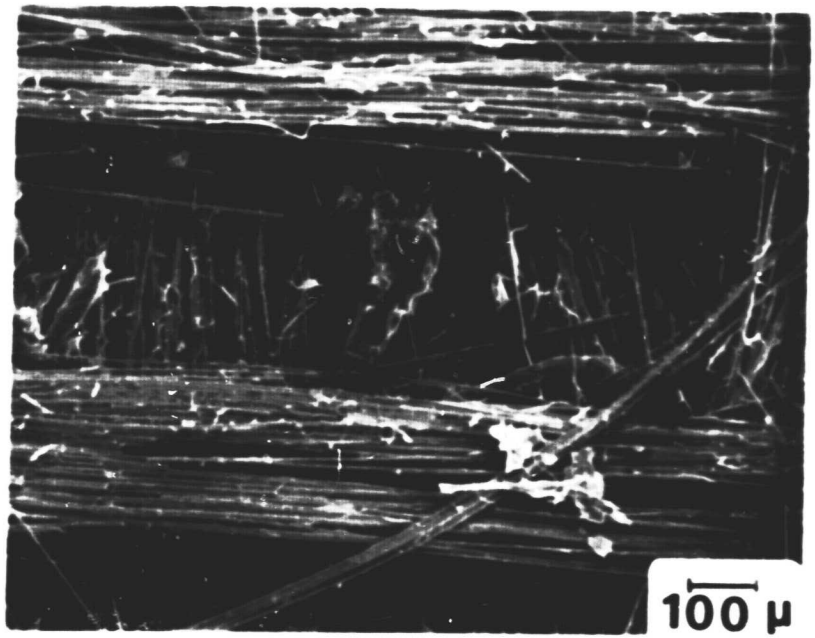

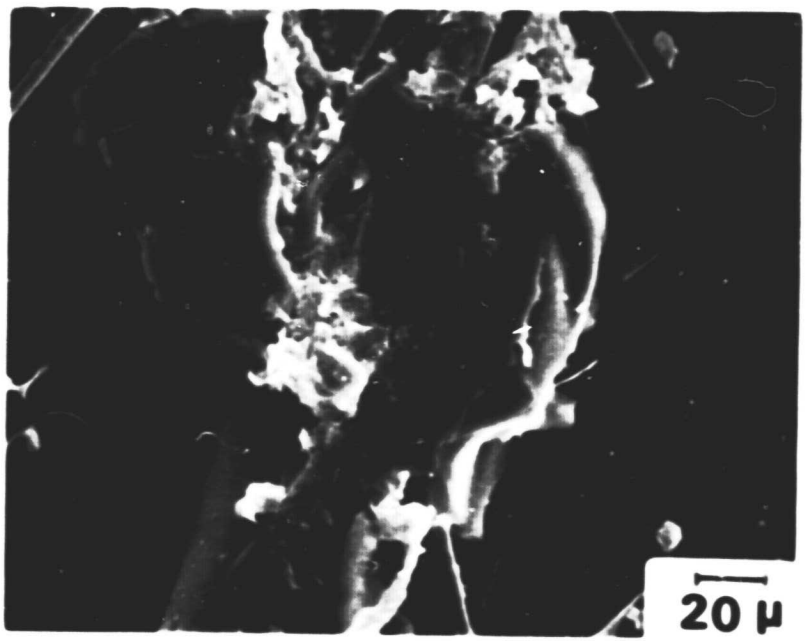

TABLE VIII

ESCA RESULTS OF FRACTURED LAP SHEAR SAMPLES [PPQ-A,RT, 450]

Sample	Photopeak	B.E. (ev)	A.F.
[PPQ-A-7, RT] No. 23	O 1s	535.0	0.17
	N 1s	400.1	0.047
	C 1s	(285.0)	0.73
	Si 2p	103.6	0.059
[PPQ-A-2, 450] No. 24	O 1s	533.1	0.12
	N 1s	399.2	0.061
	C 1s	(285.0)	0.82
[PPQ-A-2, 450] No. 60	O 1s	532.9	0.092
	N 1s	399.0	0.049
	Ca $2p_{3/2}$	349.2	0.0068
	C 1s	(285.0)	0.83
	Si 2s	154.9	0.024

energy than for PPQ. The absence of a Ti $2p_{3/2}$ photopeak is additional confirmation of cohesive failure.

The ESCA analysis of the E Glass Cloth [Style 112, A1100 Finish] is shown in Table IX. In addition to the Si 2s and O 1s photopeaks, a small but significant N 1s photopeak at 400.8 ev is also observed.

2. Polyphenylquinoxaline-chromic acid anodize - 450° [PPQ-A-2, 450] - The optical photomicrograph of this sample was similar to that for the room temperature sample above. A cohesive failure mode was assigned to this sample. SEM photomicrographs of the circular sample are shown in Figures 6 A-C. The fibers appear dewetted (Fig. 6 A), but their overall orientation is still intact. The coating on the fibers appears to be peeling off (Figs. 6 A,6 B). Plastic flow lines are observed in the adhesive as noted by the arrows in Figs. 6 B, 6 C.

The ESCA results are listed in Table VIII. Runs No. 24 and No. 60 represent different punches of the same sample. The sample for Run No. 24 had more metal showing and the sample for Run No. 60 showed mostly scrim cloth. No narrow scan Si 2s photopeak was obtained on Run No. 24. A trace Ca signal was noted in Run No. 60 along with a Si signal. It is consistent for cohesive failure that no Ti $2p_{3/2}$ photopeak was observed.

3. Polyphenylquinoxaline - phosphate/fluoride (Boeing) - room temperature [PPQ-D-5, RT] - The 35 mm photograph of the above sample is shown in Figure 7 A. An interfacial failure mode is assigned in this case based on the appearance of the adherend substrate on one member. The optical photomicrographs of samples punched from the metal failure or bare surface and the adhesive failure or covered surface are shown in Figure 7 B and 7 C, resp. The scrim cloth is visible in Fig. 7 C but it not seen in Fig. 7 B. When the covered member was punched, the adhesive broke cleanly away from the adherend.

TABLE IX

ESCA ANALYSIS OF E GLASS CLOTH AND No. 101 ALUMINUM POWDER

Photopeak	B.E. (ev)	A.F.
E-Glass		
C 1s	532.9	0.29
N 1s	400.8	0.040
C 1s	285.0	0.56
Si 2s	154.4	0.11
No. 101 Aluminum Powder		
O 1s	531.9	0.28
C 1s	285.0	0.50
Al 2s	119.8	0.21

Figure 6.

SEM photomicrographs of fractured surface of [PPQ-A-2, 450] at 190X (A), at 950X (B) and 9500X (C).

Figure 6. SEM photomicrographs of fractured surfaces of [PPQ-A-2, 450] at 190X (A), at 950X (B) and 9500X (C).

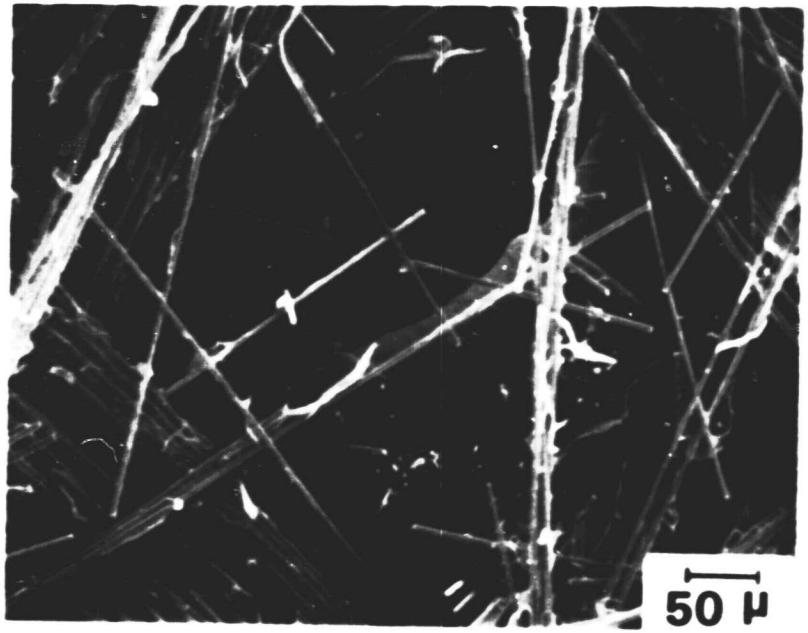

A

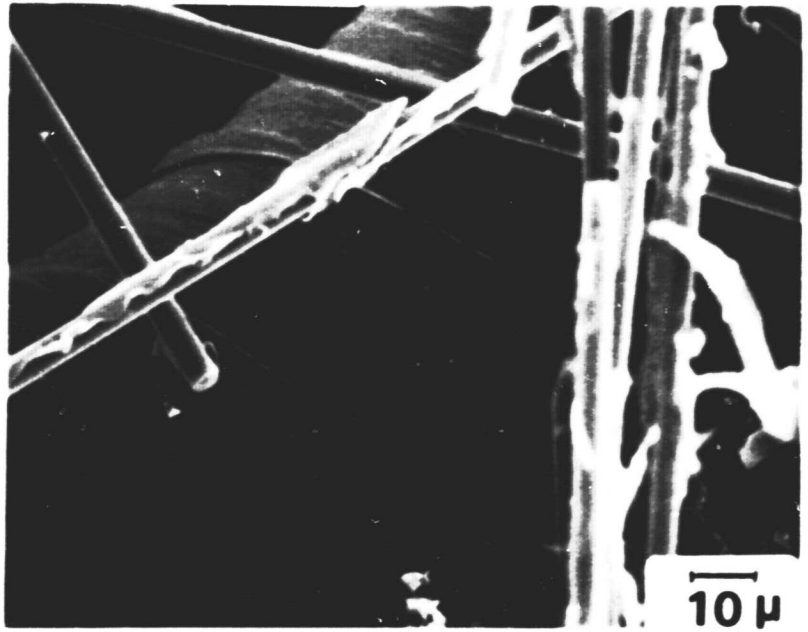

B

C

Figure 7.

Photomicrographs of [PPQ-D-5, RT]
(A) original lap shear specimen (2.5X),
(B) punched SEM/ESCA sample (13X) from
metal failure surface and (C) punched
SEM/ESCA sample (14X) from adhesive
failure surface.

Figure 7. Photomicrographs of [PPQ-D-5, RT] (A) original lap shear specimen (2.5X), (B) punched SEM/ESCA sample (13X) from metal failure surface and (C) punched SEM/ESCA sample (14X) from adhesive failure surface.

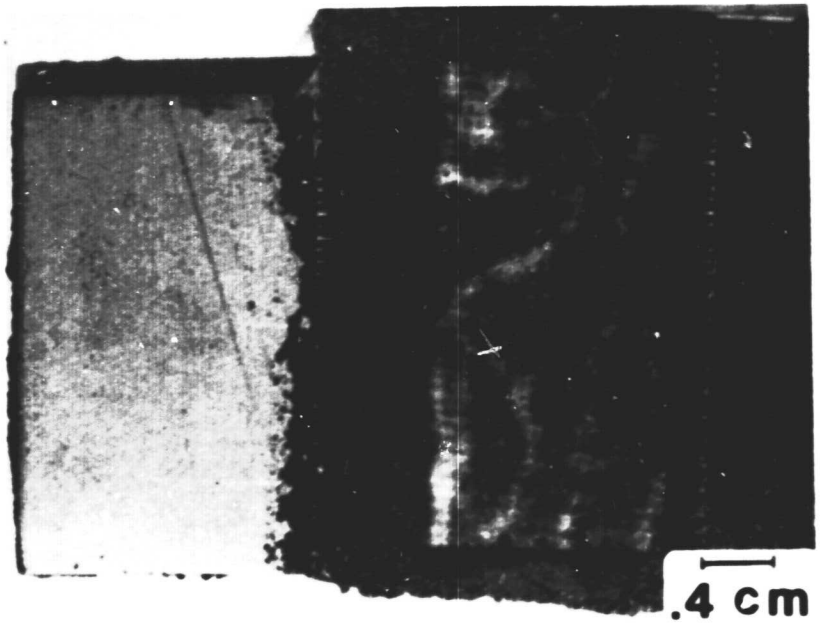

A

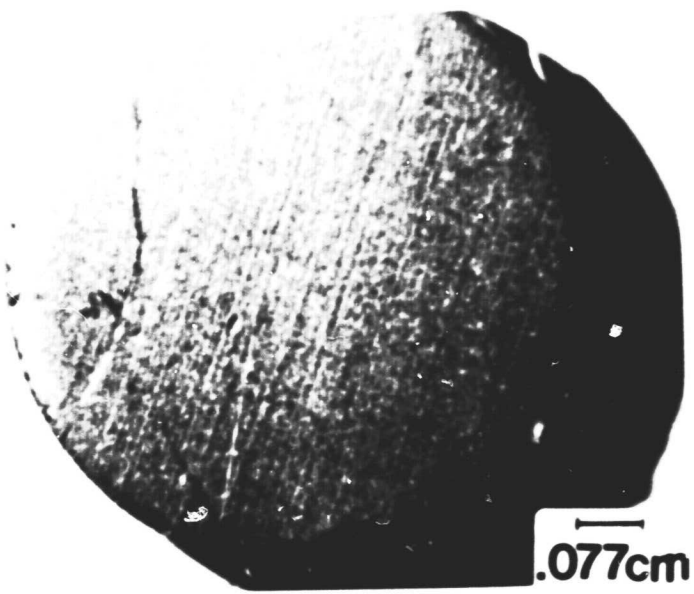

B

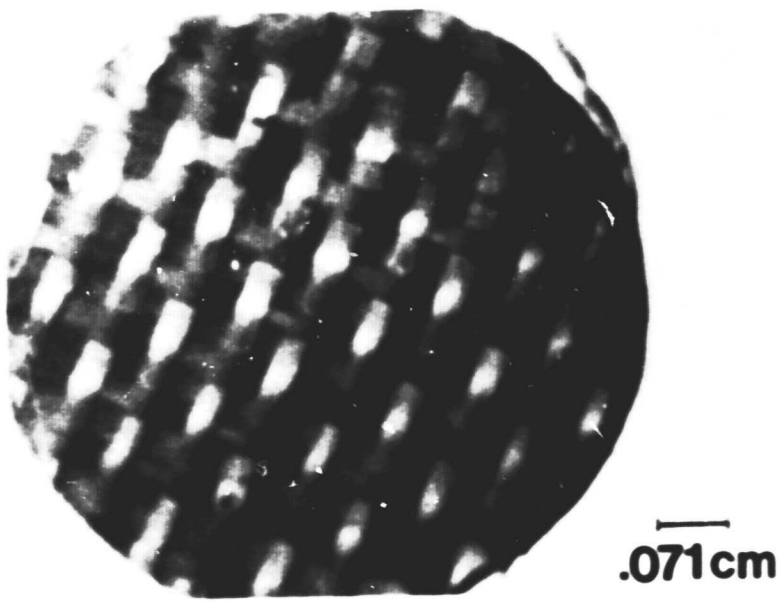

C

Thus two additional surfaces were produced, the so-called adhesive substrate surface and the metal substrate surface. A schematic diagram of this fractured lap shear specimen is shown in Figure 8. The optical photomicrographs of the adhesive and metal substrate surfaces are shown in Figures 9 A and 9 B,resp. Similar features are seen in these figures as can be seen in Figs. 7 B and 7 C.

The SEM photomicrographs of the four surfaces schematically pictured in Fig. 8 are shown in Figures 10-12. The metal failure surface in Figure 10 A shows features including the β-phase characteristic of the phosphate-fluoride [Boeing] etched surface (see Fig. 2 A). Some remnants of the primer/adhesive are noted in Figure 10 B. At the highest magnification shown in Figure 10 C, subgranular features are noted.

SEM photomicrographs of the metal substrate surfaces are shown in Figures 11 A and 11 B. The metal substrate (Fig. 11 A) and the metal failure surface (Fig. 10 A) appear quite similar. No residual primer/adhesive was noted on the metal substrate surfaces in this case however. Calcium and silicon are detected in the EDAX spectrum of the metal failure surface as shown in Fig. 11 C. Subgranular features are again noted in the higher magnification photomicrograph in Fig. 11 B. Vanadium was detected in the EDAX spectrum of the β-phase as shown in Fig. 11 D.

The SEM photomicrographs of the adhesive failure surfaces are shown at two magnifications in Figures 12 A and 12 B. No glass fibers are visible and the adhesive surface clearly shows the imprint of the metal substrate. For example, compare the features seen in Fig. 12 A with Fig. 11 A and in Fig. 12 B with Fig. 11 B. The micro voids apparent in Fig. 12 A are places where the β-phase pulled away during fracture.

The SEM photomicrographs of the adhesive substrate surface are shown at two magnifications in Figures 12 C and 12 D. Again, no glass fibers

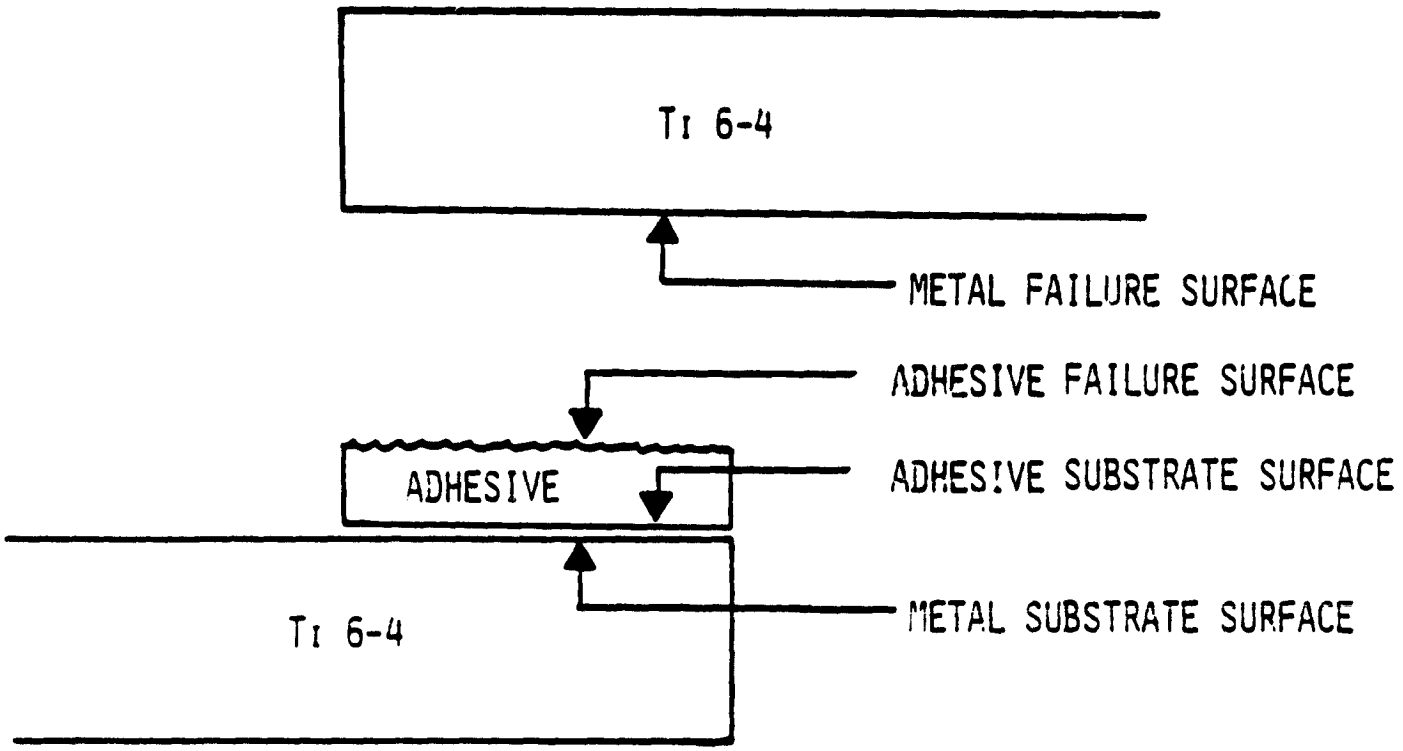

Figure 8. Schematic of fractured lap shear specimen

Figure 9.

Photomicrographs of punched SEM/ESCA samples of (A) adhesive substrate surface (14X) and (B) metal substrate surface (14X).

Figure 9. Photomicrographs of punched SEM/ESCA samples of (A) adhesive substrate surface (14X) and (B) metal substrate surface (14X).

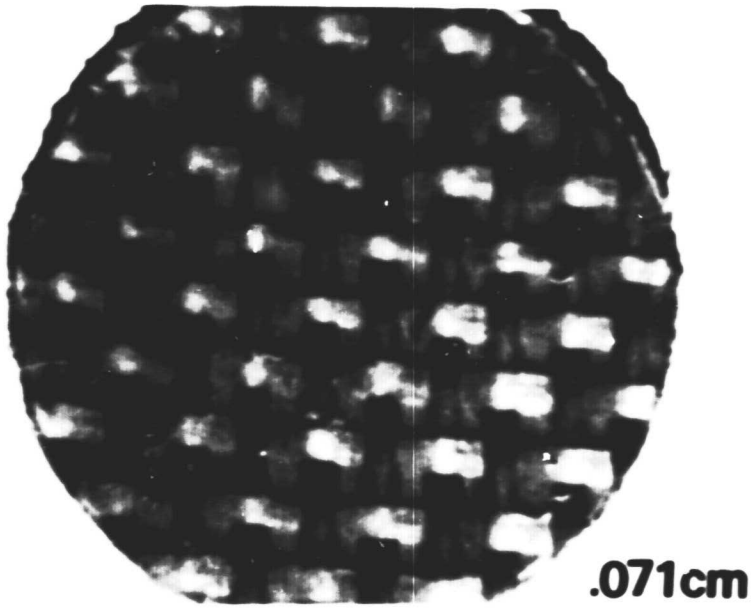

A

B

Figure 10.

SEM photomicrographs of the metal failure surface for [PPQ-D-5, RT] at 1,000X (A), 2,000X (B) and 20,000X (C).

Figure 10. SEM photomicrographs of the metal failure surface for [PPQ-D-5, RT] at 1,000X (A), 2,000X (B) and 20,000X (C).

Figure 11.

SEM photomicrographs of the metal substrate surface for [PPQ-D-5, RT] at 1,000X (A) with EDAX spectrum (B) and at 10,000X (C) with EDAX spectrum (D).

Figure 11. SEM photomicrographs of the metal substrate surface for [PPQ-D-5, RT] at 1,000X (A) with EDAX spectrum (B) and at 10,000X (C) with EDAX spectrum (D).

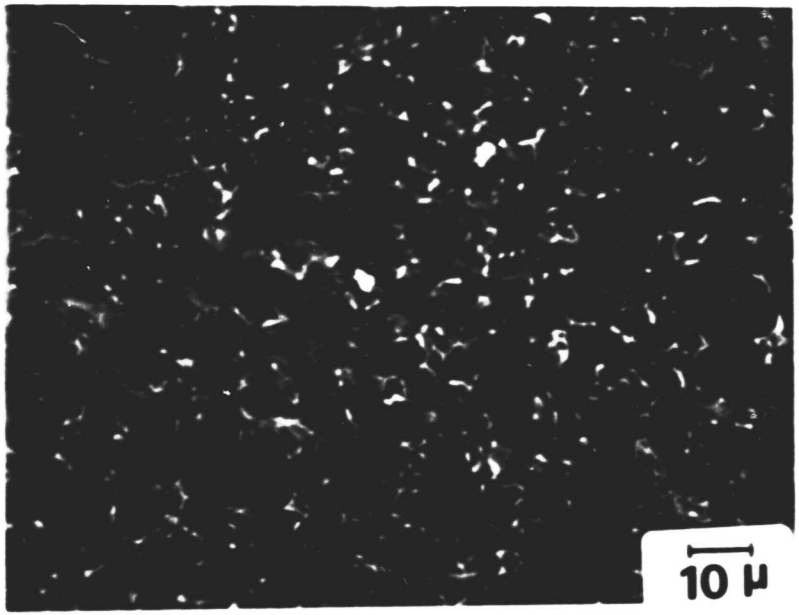

A

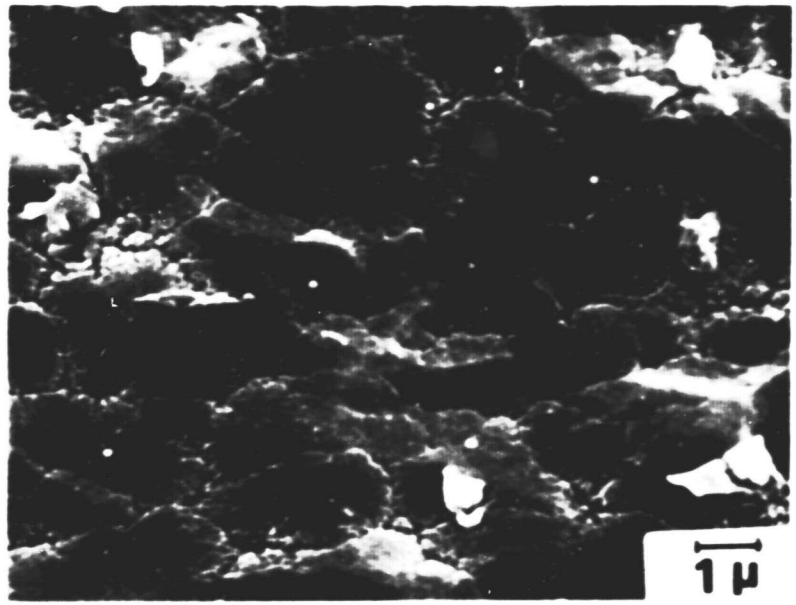

B

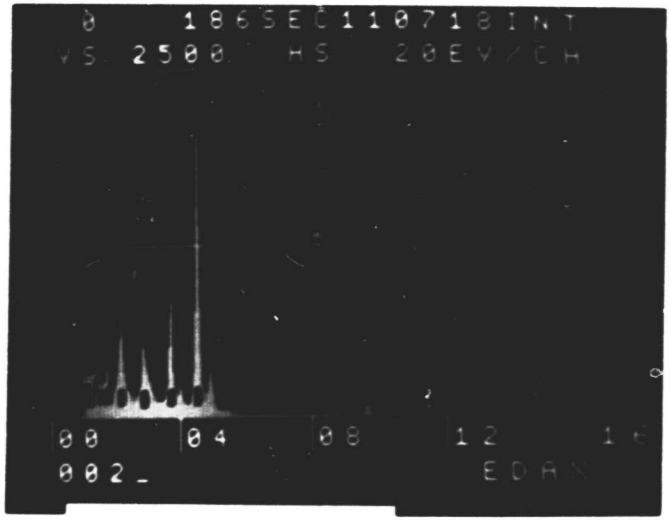

C Mg Al Si Au Pd Ca Ti

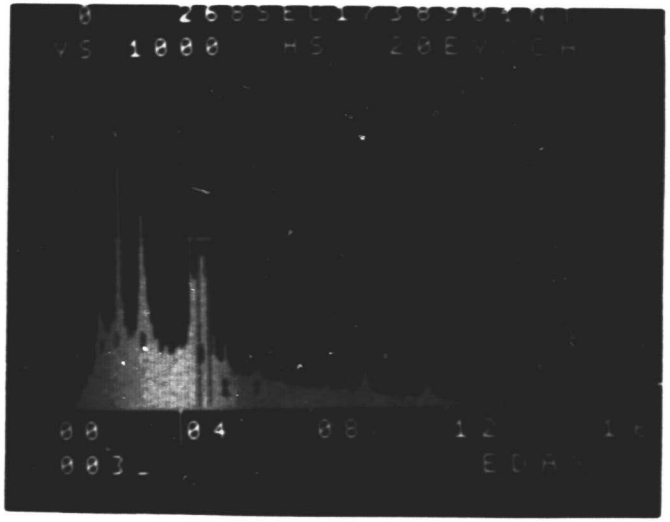

D Al Au Pd Ti V Fe Au

Figure 12.

SEM photomicrographs of the adhesive failure surface for [PPQ-D-5, RT] at 1,000X (A) and 20,000X (B) and of the adhesive substrate surface for [PPQ-D-5, RT] at 475X (C) and 9,500X (D).

Figure 12. SEM photomicrographs of the adhesive failure surface for [PPQ-D-5, RT] at 1,000X (A) and 20,000X (B) and of the adhesive substrate surface for [PPQ-D-5, RT] at 475X (C) and 9,500X (D).

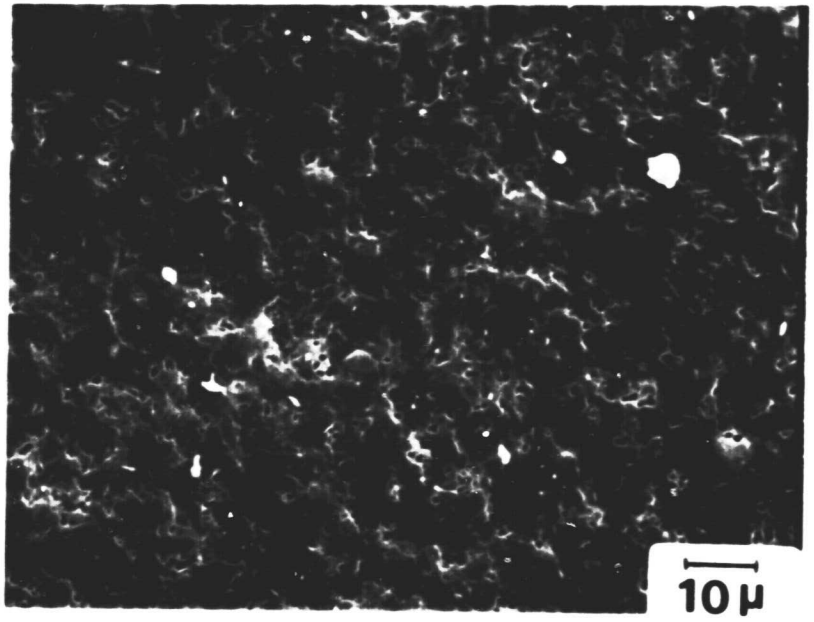

A

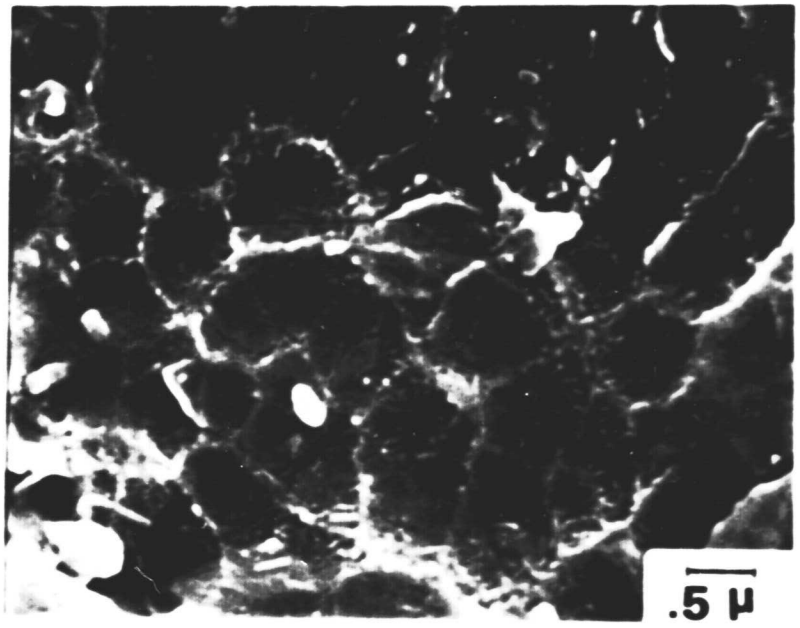

B

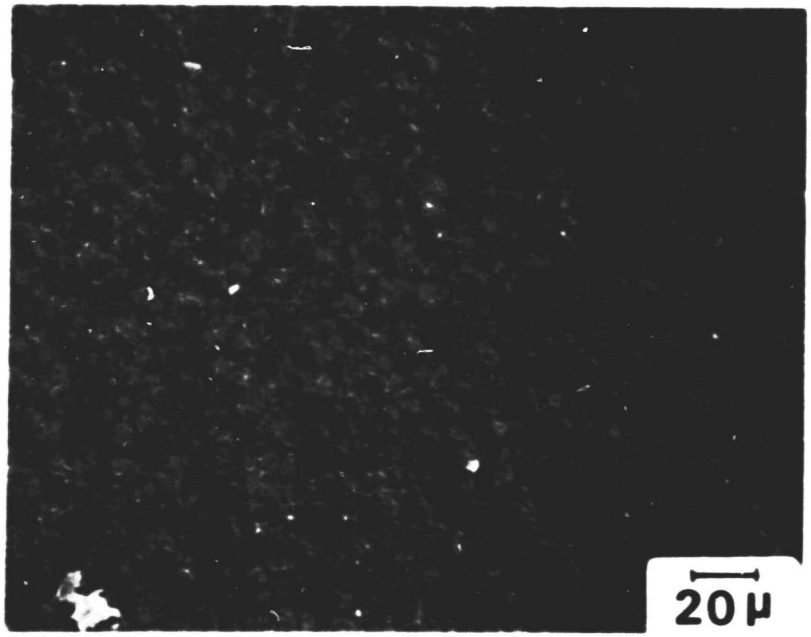

C

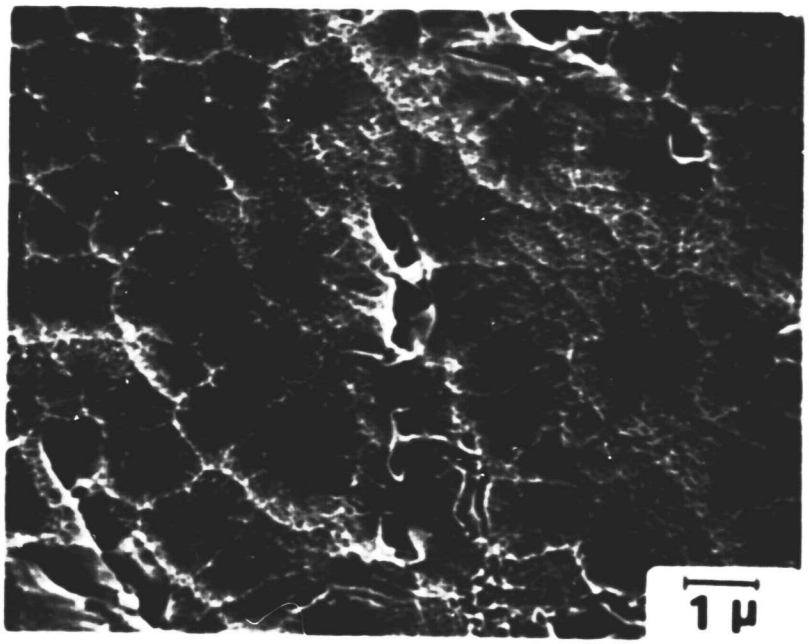

D

are seen and the imprint of the metal substrate on the adhesive is seen. The holes corresponding to the location of the β-phase before fracture are clearly seen in Fig. 12 D. Subgranular features are seen in both Figs. 12 B and 12 D.

The ESCA results of the four surfaces discussed above are shown in Table X. The metal failure surface (Fig. 10 A) shows a significant Ti signal which fact is further confirmation of the assignment of interfacial failure for this sample. The photopeak at a binding energy of 530.5 ev is assigned to oxygen in the surface oxide layer. We have reported (14) a value of 530.5 ev for the O 1s photopeak following a phosphate-fluoride treatment of Ti 6-4. Thus, the ESCA results support the existence of a titanium oxide layer on the metal failure surface. The presence of Ca is consistent with the results in Table VI where Ca was observed as a residual on the Ti 6-4 adherend surface after the phosphate-fluoride treatment. The N 1s photopeak at 399.3 ev is consistent with the N 1s photopeak observed for the Ti 6-4 adherend surface after any chemical pretreatment (see Table VI). However, the origin of the nitrogen is not clear since a N 1s photopeak at about the same binding energy is observed for both pretreated Ti 6-4 and PPQ (see Table VII). The observation of a significant Si 2s photopeak is quite interesting. Again, the origin of this Si signal is not clear. However, the fact that failure occurred at this interface may be associated with the presence of silicon. The SEM photomicrographs (see Fig. 10 A) shows no evidence of glass fragment from the scrim cloth. It is known that the scrim cloth is coated with an organo-silicon compound. Does in fact degradation and subsequent migration of silicon-containing compounds to the interface occur? The answer to this question will involve additional experiments.

The adhesive failure surfaces give an O 1s photopeak at 532.7 ev

TABLE X

ESCA RESULTS OF FRACTURED LAP SHEAR SAMPLE [PPQ-D-5, RT]

Surface Analyzed	Photopeak	B.E.(ev)	A.F.
Metal Failure Surface No. 38	O 1s	530.5	0.27
	Ti $2p_{3/2}$	458.9	0.044
	N 1s	399.3	0.022
	Ca $2p_{3/2}$	347.5	0.0078
	C 1s	(285.0)	0.60
	Si 2s	153.5	0.052
Adhesive Failure Surface No. 34	O 1s	532.7	0.13
	N 1s	399.3	0.050
	C 1s	(285.0)	0.79
	Si 2s	153.6	0.031
Metal Substrate Surface No. 58	O 1s	530.2	0.27
	V $2p_{3/2}$	515.1	0.0020
	Ti $2p_{3/2}$	458.9	0.070
	N 1s	399.4	0.020
	Ca $2p_{3/2}$	347.5	0.012
	C 1s	(285.0)	0.62
	Pb $4f_{7/2}$	139.0	0.0081
Adhesive Substrate Surface No. 59	O 1s	533.2	0.071
	Ti $2p_{3/2}$	459.6	0.0037
	N 1s	399.0	0.057
	C 1s	(285.0)	0.87
	Pb $4f_{7/2}$	138.7	0.0014

(see Table X) characteristic of PPQ (see Table VII). Again, a significant Si signal is observed on this surface where no glass fibers are seen (see Fig. 12 A). The absence of a Ti photopeak is additional confirmation of interfacial failure. A further conclusion can be drawn. Failure occurred at the primer/oxide interface rather than in the oxide layer in which case a Ti signal should have been observed.

The metal substrate surface (see Figs. 8, 9 B, 11) shows an O 1s photopeak at 530.2 ev characteristic of the pretreated Ti 6-4. In this case a small V peak and a significant Ti peak were detected. The presence of Ca is consistent with the composition of a phosphate-fluoride treated Ti 6-4 surface. The presence of a trace quantity of lead on this surface and on the adhesive substrate surface is not explained.

The adhesive substrate surface (see Figs. 8, 9 A, 12 C, 12 D) shows an O 1s photopeak at 533.2 ev characteristic of PPQ. A small Ti peak was detected here indicative of fracture of the oxide layer. No silicon was noted on either of these substrate surfaces.

4. Polyphenylquinoxaline - phosphate/fluoride (Boeing) - 450° [PPQ-D-4, 450]. - A cohesive failure was assigned in this case based on similar optical photomicrographs (see Figs. 5 A, 5 B). The SEM photomicrographs of this sample were similar to the one shown in Fig. 5 C and so are not repeated here. Punching out the ESCA samples did again cause separation between the adhesive and substrate on both members as depicted in Fig. 8.

The ESCA results for this sample are listed in Table XI. The O 1s photopeak is characteristic of PPQ. Also, both Ca and Si are observed on this surface which is consistent with cohesive failure resulting in exposed scrim cloth thus reflecting the glass composition.

The sample separated when punched and the SEM photomicrograph of the adhesive substrate surface (see Fig. 8) appeared similar to the one shown

TABLE XI

ESCA RESULTS OF FRACTURED LAP SHEAR SAMPLE [PPQ-D-4, 450]

Surface Analyzed	Photopeak	B.E.(ev)	A.F.
Adhesive Failure Surface No. 37	O 1s	533.0	0.14
	N 1s	398.9	0.044
	Ca $2p_{3/2}$	348.5	0.011
	C 1s	(285.0)	0.76
	Si 2s	154.0	0.039
Adhesive Substrate Surface	O 1s	533.3	0.33
	Ti $2p_{3/2}$	460.8	0.0032
	N 1s	399.4	0.033
	C 1s	(285.0)	0.63
	Pb $4f_{7/2}$	139.0	0.0010
Metal Substrate Surface	O 1s	530.6	0.28
	V $2p_{3/2}$	516.0	0.0010
	Ti $2p_{3/2}$	458.8	0.057
	N 1s	399.3	0.012
	Ca $2p_{3/2}$	347.5	0.0061
	C 1s	(285.0)	0.64
	Pb $4f_{7/2}$	138.8	0.0034

in Fig. 12C. The EDAX spectrum showed both Ti and Al. The SEM photomicrographs of the metal substrate surface (see Fig. 8) appeared similar to the one shown in Fig. 11 A. The ESCA results of these two surfaces are shown in Table XI. The adhesive substrate surface shows a minimal Ti signal suggesting oxide transfer. The O 1s photopeak is consistent with PPQ(see Table VII). The metal substrate surface shows a significant Ti signal indicative of minimal primer/adhesive transferred to substrate. The O 1s photopeak at 530.6 ev is characteristic of the oxide and not PPQ.

D. Fractured Lap Shear Samples - PPQ Mod I

1. Polyphenylquinoxaline Mod I - chromic acid anodize - room temperature [PPQ M1-A-7, RT] - The 35 mm photograph of this sample in Figure 13 A shows mixed (interfacial and cohesive) mode failure. A representative sample was punched as shown in the optical photomicrograph in Fig. 13 B. The SEM photomicrographs in Figs. 13 C and 13 D show a cohesive failure region. The glass fibers still appear wetted and their orientation intact. The polymer portion (Fig. 13 D) has a high surface area. The interfacial failure region is shown in Figures 14 A-C. The light areas in Fig. 14 A appear to result from a residual primer/adhesive film covering the Ti 6-4 substrate. This film is shown at higher magnification in Fig. 14 B. The high magnification SEM photomicrograph in Fig. 14 C taken in a dark area (Fig. 14 A) is representative of an anodized Ti 6-4 substrate.

The ESCA results for the sample are listed in Table XII. Run Nos. 25, 30 and 63 represent different punches of the same sample. The sample for Run No. 30 showed about half metal/half scrim cloth; the sample for Run No. 25 was taken from the metal section; and the sample for Run No. 63 showed about half metal/half scrim cloth. The oxygen 1s photopeak at 533.6 ev for Run Nos. 30 and 63 is characteristic of PPQ (see Table VII). Calcium and silicon result from glass fibers being exposed on fracture.

Figure 13.

Photomicrographs of [PPQM1-A-7, RT]
(A) original lap shear specimen (2X),
(B) punched SEM/ESCA sample (14X),
(C) SEM/fracture surface (200X) and
(D) SEM/fracture surface (5,000X).

Figure 13. Photomicrographs of [PPQM1-A-7, RT] (A) original lap shear specimen (2X), (B) punched SEM/ESCA sample (14X), (C) SEM/fracture surface (200X) and (D) SEM/fracture surface (5,000X).

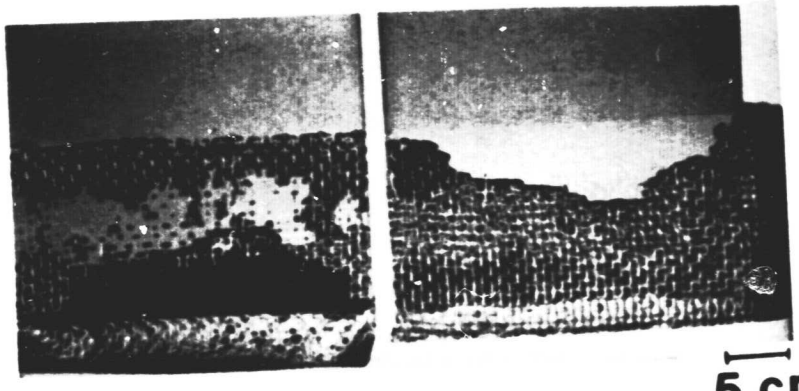

A

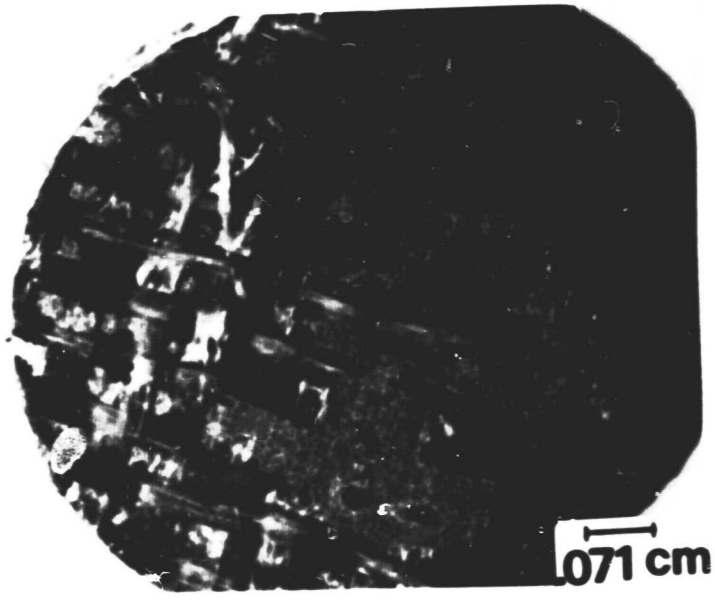

B

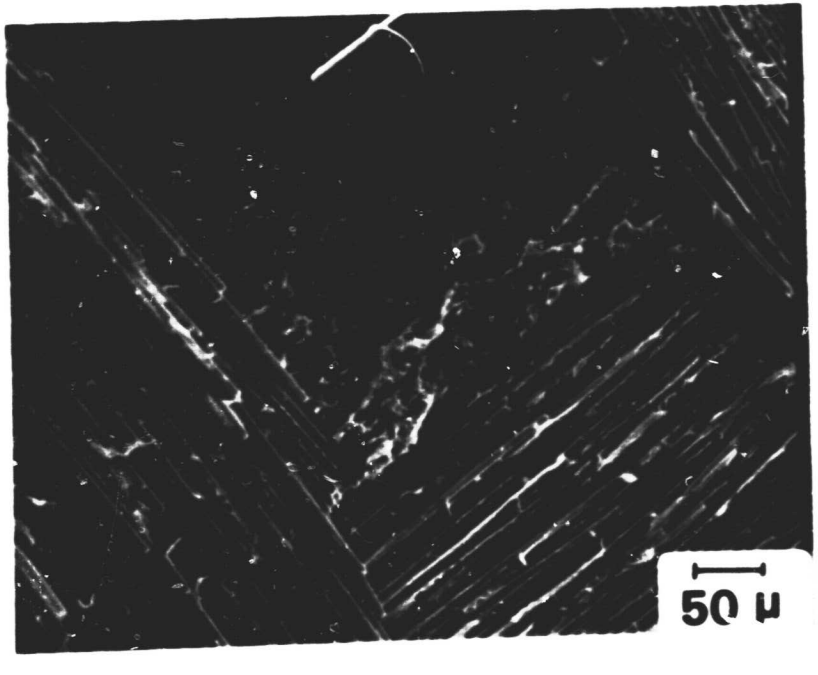

C

D

Figure 14.

SEM photomicrographs of [PPQM1-A-7, RT] showing light and dark areas at 200X (A), light area at 1,000X (B) and dark area at 9,500X (C).

Figure 14. SEM photomicrographs of [PPQM1-A-7, RT] showing light and dark areas at 200X (A), light area at 1,000X (B) and dark area at 9,500X (C).

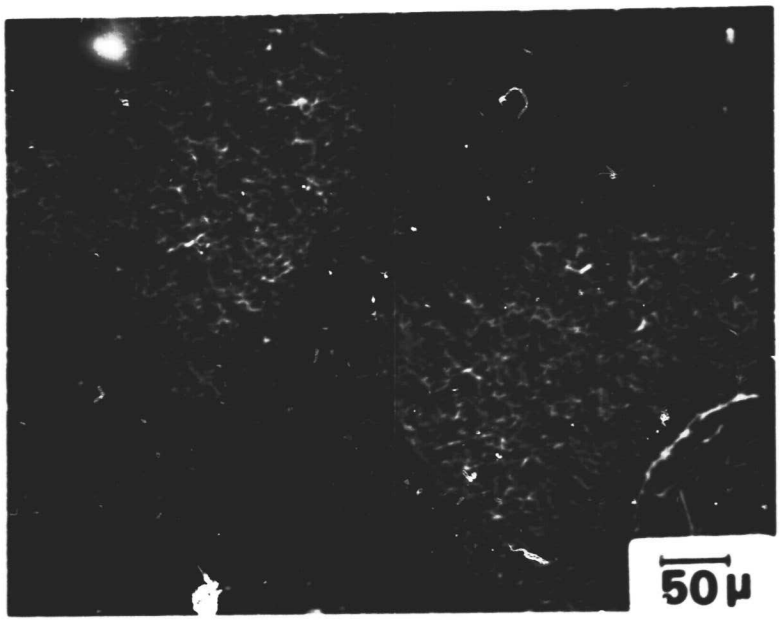

A

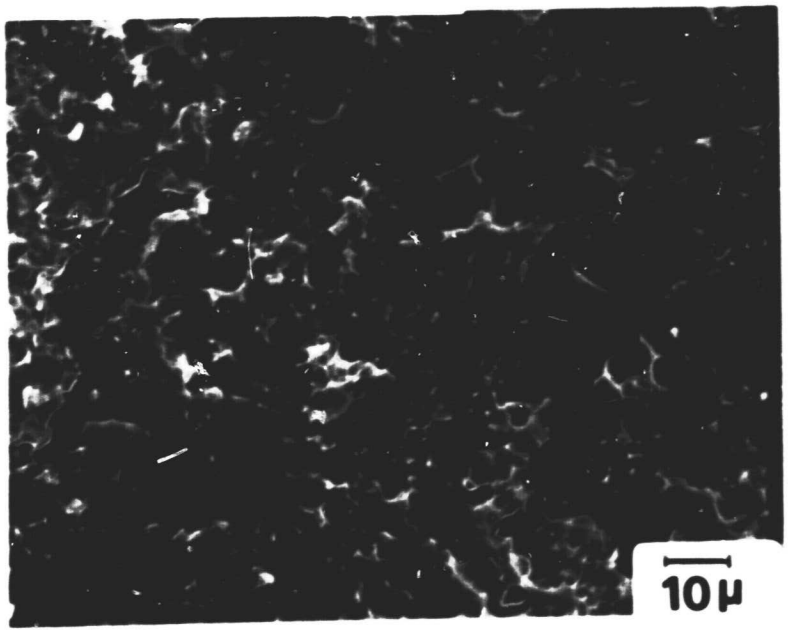

B

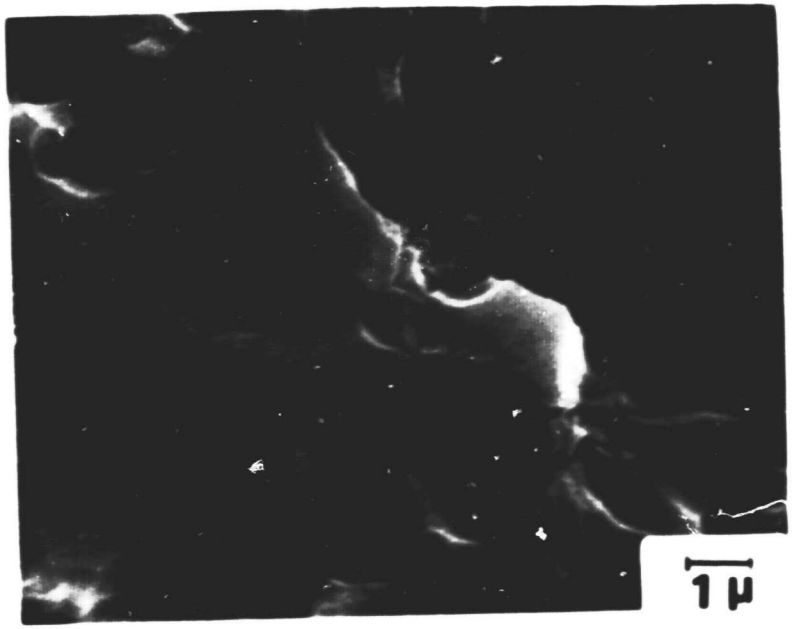

C

TABLE XII

ESCA RESULTS OF FRACTURED LAP SHEAR SAMPLES [PPQM1-A, RT, 450]

Sample	Photopeak	B.E.(ev)	A.F.
[PPQM1-A-7, RT] No. 30	O 1s	533.6	0.12
	N 1s	399.3	0.054
	Ca $2p_{3/2}$	349.7	0.0074
	C 1s	(285.0)	0.78
	Si 2p	104.7	0.035
[PPQM1-A-7, RT] No. 25	O 1s	530.8	0.12
	Ti $2p_{3/2}$	458.9	0.022
	N 1s	399.3	0.041
	C 1s	(285.0)	0.81
[PPQM1-A-7, RT] No. 63	O 1s	533.2	0.073
	N 1s	399.2	0.056
	Ca $2p_{3/2}$	349.1	0.0029
	C 1s	(285.0)	0.85
	Si 2p	104.2	0.018
	Pb $4f_{7/2}$	139.5	0.0002
[PPQM1-A-4, 450] No. 26	O 1s	533.5	0.10
	N 1s	399.1	0.058
	C 1s	(285.0)	0.84

The absence of a Ti signal suggests a thin residual primer/adhesive film with a minimal (<10%) area of exposed substrate. However, for Run No. 25, a significant Ti signal was noted and the O 1s photopeak at 530.8 ev is characteristic of the metal oxide layer which suggests interfacial failure in this region. Surprisingly, no boron signal was detected on any of the samples.

2. Polyphenylquinoxaline Mod I - chromic acid anodize - 450° [PPQMI-A-4, 450] - The 35 mm photograph and optical photomicrograph of this sample in Figures 15 A and 15 B show again mixed mode failure. The SEM photomicrographs in Fig. 15 C and 15 D show a cohesive failure region. Glass fibers are seen and the adhesive shows considerable deformation with a large amount of surface area. The SEM photomicrographs of the interfacial failure region were similar to those of PPQ-A-7, RT. The ESCA results for this sample are listed in Table XII. The O 1s photopeak is characteristic of PPQ. Again, no boron signal was observed.

3. Polyphenylquinoxaline Mod I - phosphate/fluoride - room temperature [PPQM1-D-5, RT] - The 35 mm photograph and the optical photomicrograph of this sample showed interfacial failure. The SEM photomicrographs shown in Figures 16 A and 16 B show the substrate surface with thin patches of primer/adhesive remaining. Sub-granular structure is noted in Fig. 16 B. The adhesive popped off the substrate when the circular sample was punched.

The ESCA results are listed in Table XIII for the different surfaces. The O 1s photopeak appears at a higher binding energy on the adhesive surface compared to the two metal surfaces. This has been a consistent observation throughout the ESCA analysis. The Ti photopeak is observed on the adhesive surface indicative of failure of the surface oxide layer. A Ca photopeak is observed on the metal surfaces resulting from the phosphate/

Figure 15.

Photomicrographs of [PPQMI-A-4, 450]
(A) original lap shear specimen (2X),
(B) punched SEM/ESCA sample (14X),
(C) SEM/fracture surface (475X) and
(D) SEM/fracture surface (9500X)

Figure 15. Photomicrographs of [PPQM1-A-4, 450] (A) original lap shear specimen (2X), (B) punched SEM/ESCA sample (14X), (C) SEM/fracture surface (475X) and (D) SEM/fracture surface (9500X).

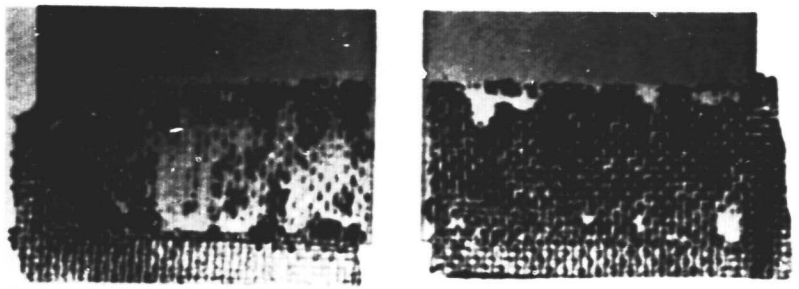

A

B

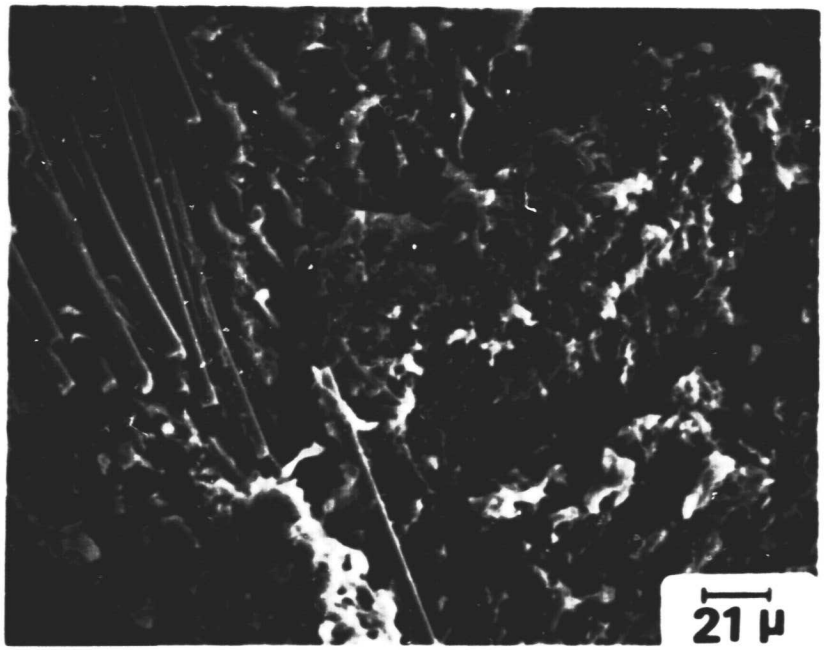

C

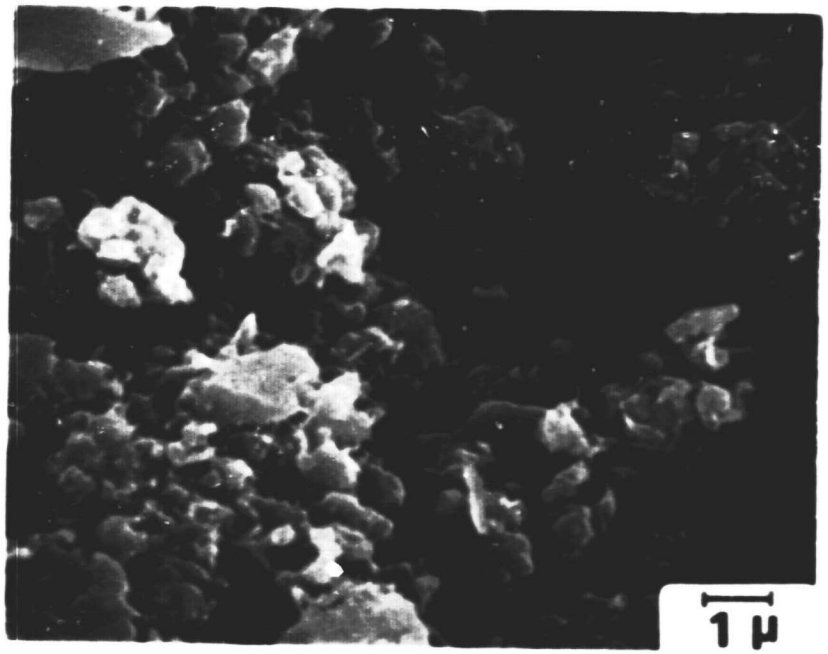

D

Figure 16.

SEM photomicrographs of [PPQM1-D-5, RT] at 100X (A) and 5,000X (B).

Figure 16. SEM photomicrographs of [PPQM1-D-5, RT] at 100X (A) and 5,000X (B).

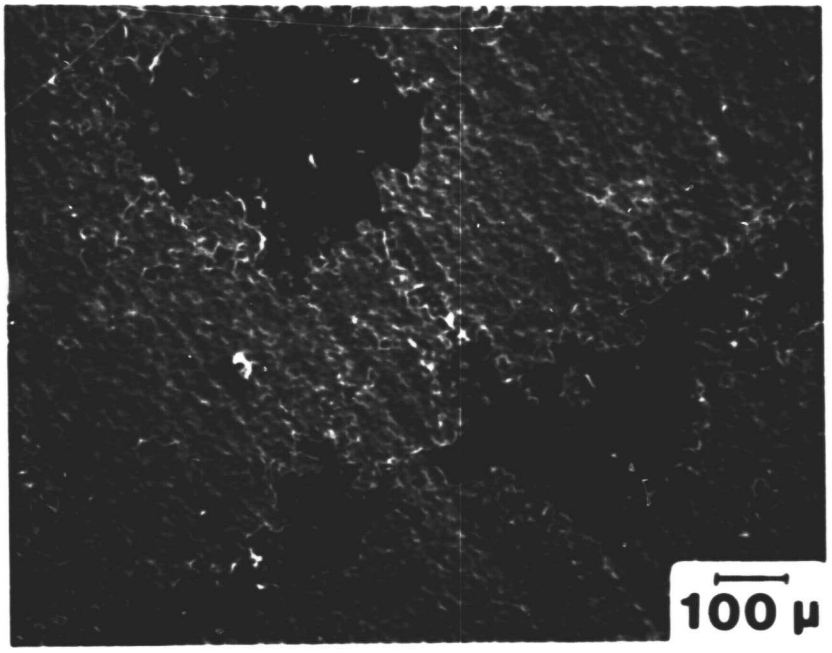

A

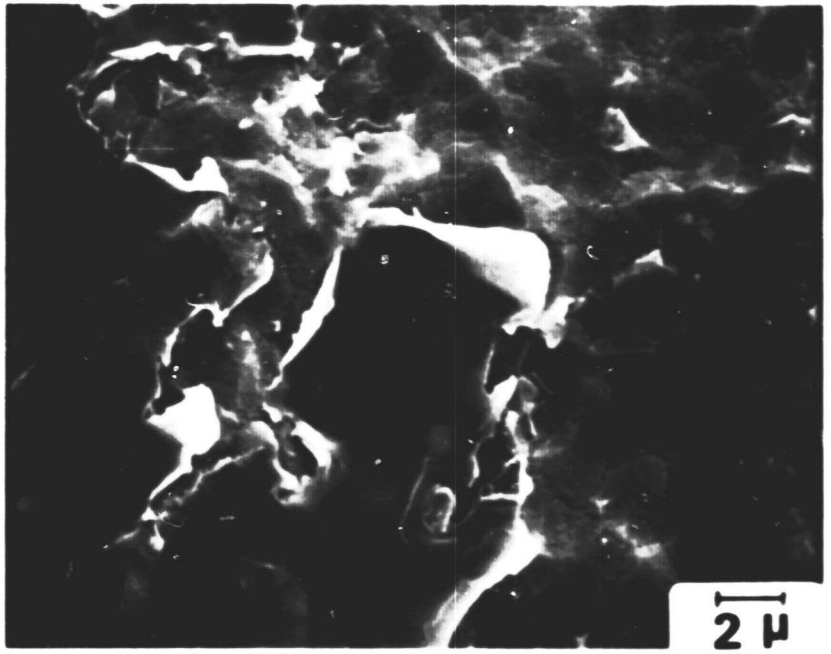

B

TABLE XIII

ESCA RESULTS OF FRACTURED LAP SHEAR SAMPLE [PPQM1-D-5, RT]

Surface Analyzed	Photopeak	B.E.(ev)	A.F.
Metal Failure Surface No. 66	Na 1s	1072.0	0.0011
	F 1s	685.1	0.0068
	O 1s	530.4	0.23
	Ti $2p_{3/2}$	458.7	0.056
	Ca $2p_{3/2}$	347.9	0.0046
	C 1s	(285.0)	0.68
	Pb $4f_{7/2}$	139.0	0.0036
	Si 2p	103.4	0.020
Metal Failure Surface No. 28	O 1s	530.3	0.26
	Ti $2p_{3/2}$	458.8	0.064
	N 1s	399.4	0.025
	Ca $2p_{3/2}$	347.6	0.0048
	C 1s	(285.0),288.5	0.61
	Pb $4f_{7/2}$	137.7	0.0032
	Si 2p	101.4	0.025
Adhesive Failure Surface No. 32	O 1s	532.0	0.16
	Ti $2p_{3/2}$	460.3	0.020
	N 1s	399.3	0.048
	C 1s	(285.0)289.4	0.75
	Si 2p	102.7	0.019

fluoride pretreatment. A Si photopeak is observed on all surfaces which reinforces the suggestion that low lap shear strengths are associated with the presence of Si in the interfacial region.

4. Polyphenylquinoxaline Mod I - phosphate/fluoride - 450° [PPQMI-D-8, 450] - The failure mode here is mixed. The adhesive showed elastic deformation with a large surface area. The SEM photomicrograph of the metal substrate appears similar to that for the room temperature sample shown in Fig. 16. Again, the adhesive popped off the substrate when punched. The ESCA results are listed in Table XIV. Again the lower binding energy of the O 1s photopeak is assigned to the surface metal oxide layer. No Ti signal is observed on the adhesive failure surface suggesting that the surface oxide layer remained intact.

E. Fractured Lap Shear Samples - L13

1. L13-chromic acid anodize-room temperature [L13-A-2, RT] - The failure mode here is mixed. The SEM photomicrographs in Figure 17 illustrate the interface between adherend and the primer/adhesive. The Al filler particles can be seen as protrusions in the adhesive. Deformation is seen only at the edges of the adhesive. There is no evidence of scrim cloth. The ESCA results are listed in Table XV. The presence of a Ti signal indicates partial interfacial failure. The presence of Si is noted but its source is unknown. The fact that no Al signal is observed suggests that the filler particles (Fig. 17) are covered with adhesive or the total exposed area of these particles is minimal.

2. L13-chromic acid anodize - 450° [L13-A-2, 450] - These samples failed cohesively and the SEM photomicrographs are shown in Figure 18. A high density of Al particles are noted. Several void areas are seen in Fig. 18 B as well as the scrim cloth. A more detailed look at the Al particles is shown in Figure 19 A. The bottom of a void area in Fig. 19 A is shown in Fig. 19 B. The Al particles tend to be small and are well covered by primer/adhesive.

TABLE XIV

ESCA RESULTS OF FRACTURED LAP SHEAR SAMPLE [PPQM1-D-8, 450]

Sample	Photopeak	B.E.(ev)	A.F.
Metal Substrate Surface No. 33	O 1s	530.4	0.28
	Ti $2p_{3/2}$	458.4	0.071
	N 1s	399.3	0.028
	Ca $2p_{3/2}$	347.7	0.010
	C 1s	(285.0)	0.61
	Pb $4f_{7/2}$	139.1	0.0049
Adhesive Failure Surface No. 31	O 1s	533.3	0.12
	N 1s	398.9	0.047
	C 1s	(285.0)	0.81
	Si 2p	103.9	0.031

Figure 17.

SEM photomicrographs of [L13-A-2, RT]
at 160X (A) and 400X (B).

Figure 17. SEM photomicrographs of [L13-A-2, RT] at 160X (A) and 400X (B).

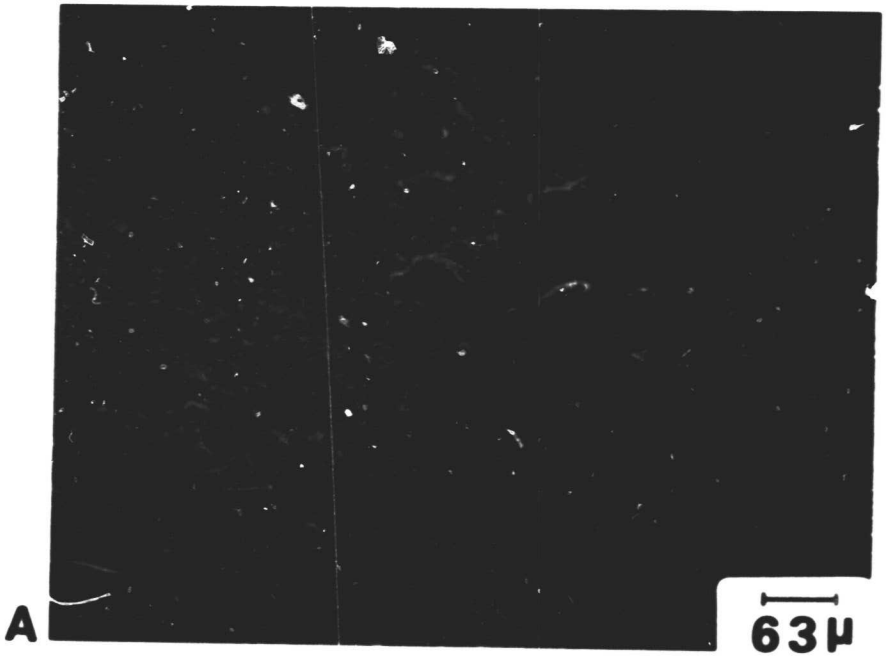
A
63μ

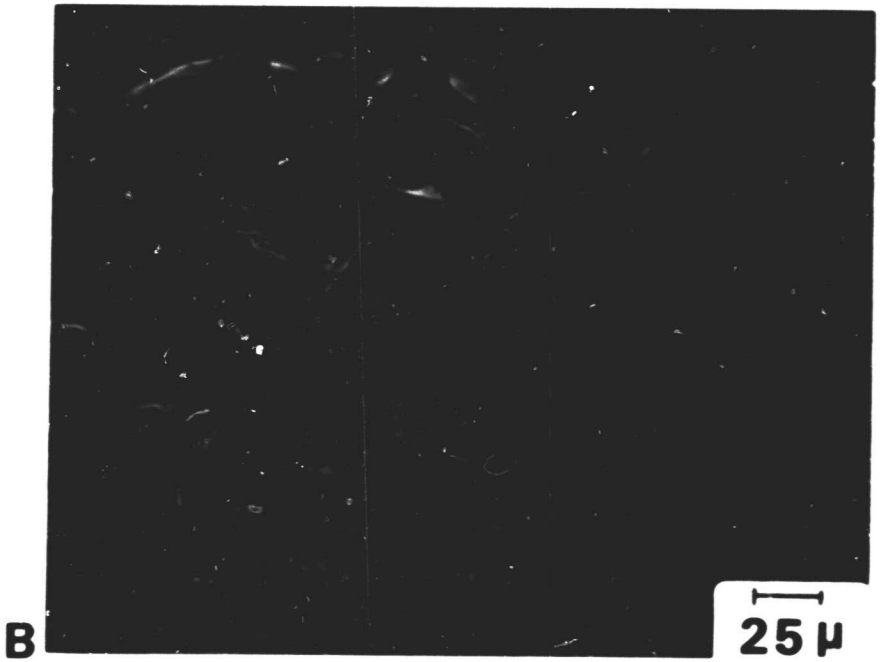
B
25μ

TABLE XV

ESCA RESULTS OF FRACTURED LAP SHEAR [L13] SAMPLES

Sample	Photopeak	B.E.(ev)	A.F.
[L13-A-2-RT] No. 14	O 1s	532.3	0.18
	V $2p_{1/2}$	523.4	0.0098
	Ti $2p_{3/2}$	459.8	0.0088
	N 1s	400.1	0.024
	C 1s	(285.0)	0.75
	Si 2p	102.4	0.027
[L13-A-2, 450] No. 15	O 1s	532.3	0.21
	N 1s	400.3	0.032
	C 1s	(285.0)	0.76
[L13-A-2, 450] No. 18	O 1s	532.1	0.21
	N 1s	400.0	0.040
	C 1s	(285.0)	0.66
	Al 2s	120.0	0.071
	Si 2p	102.4	0.021
[L13-D-5, RT] Adhesive Failure Surface No. 20	O 1s	532.1,538.3	0.13
	Ti $2p_{3/2}$	459.4	0.0032
	N 1s	400.7	0.042
	C 1s	(285.0)	0.82
[L13-D-5, RT] Metal Substrate Surface No. 21	O 1s	530.6, 531.9	0.26
	Ti $2p_{3/2}$	458.4	0.081
	N 1s	400.5	0.027
	C 1s	(285.0)	0.63
[L13-D-6, 450] No. 19	O 1s	531.7	0.33
	Ti $2p_{3/2}$	458.8	0.063
	N 1s	400.7	0.026
	Ca $2p_{3/2}$	347.0	0.0048
	C 1s	(285.0)	0.58

Figure 18.

SEM photomicrographs of [L13-A-2, 450]
at 40X (A) and 160X (B).

Figure 18. SEM photomicrographs of [L13-A-2, 450] at 40X (A) and 160X (B).

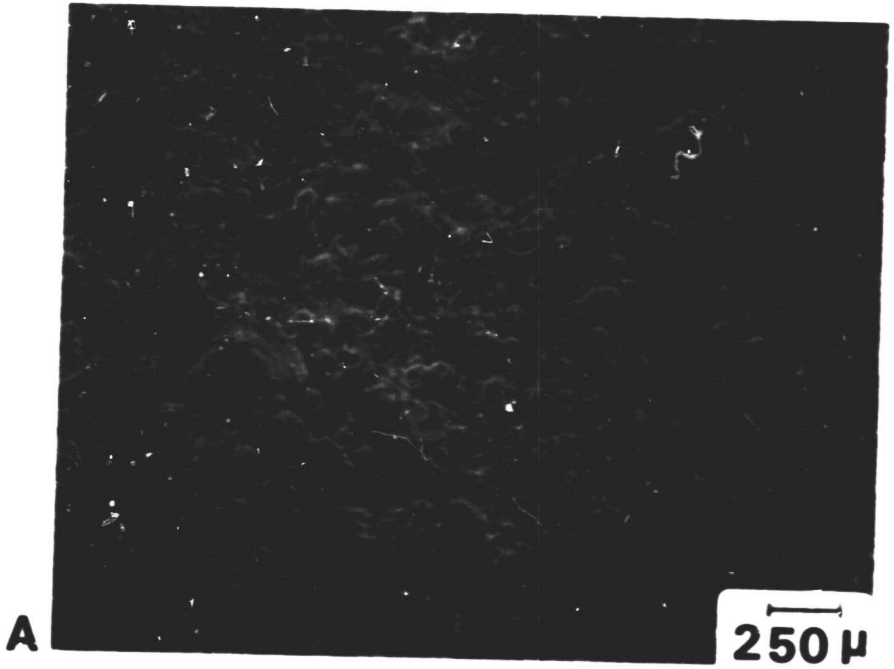
A
250 µ

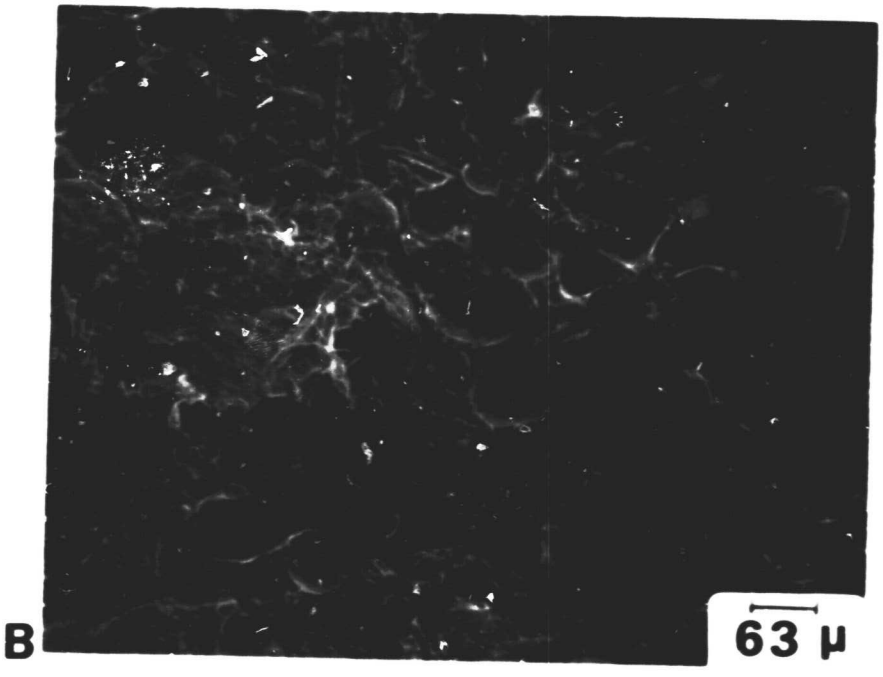
B
63 µ

Figure 19.

SEM photomicrographs of [L13-A-2, 450]
at 50X (A), at 300X (B) and at 500X (C).

Figure 19. SEM photomicrographs of [L13-A-2, 450] at 50X (A), at 500X (B) and at 500X (C).

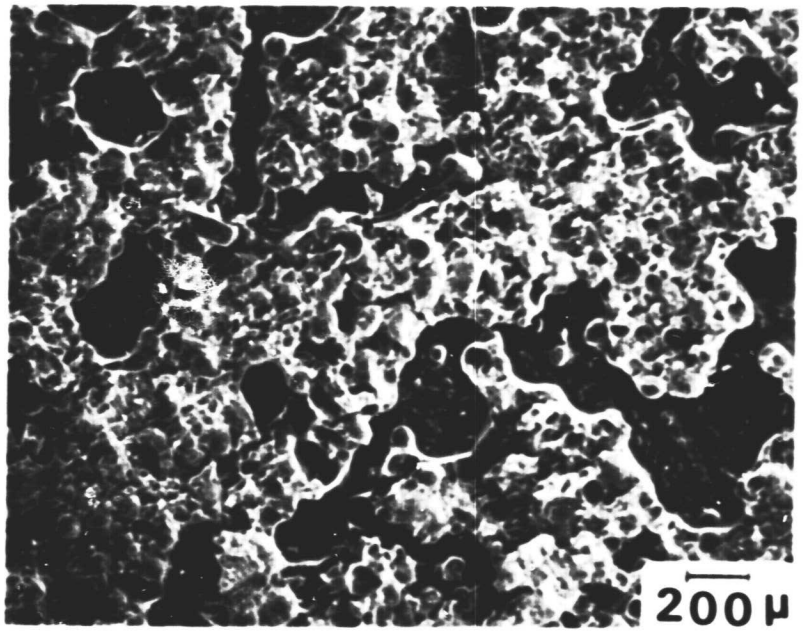

A

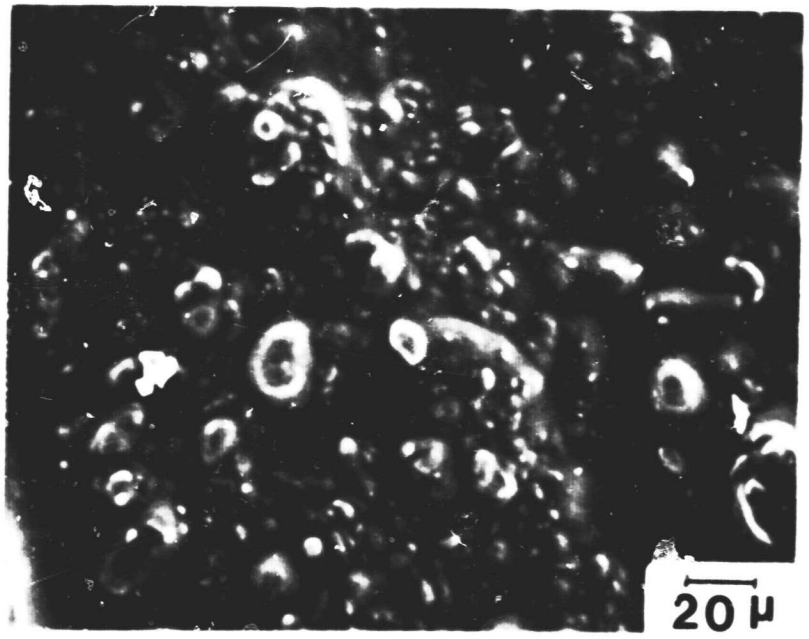

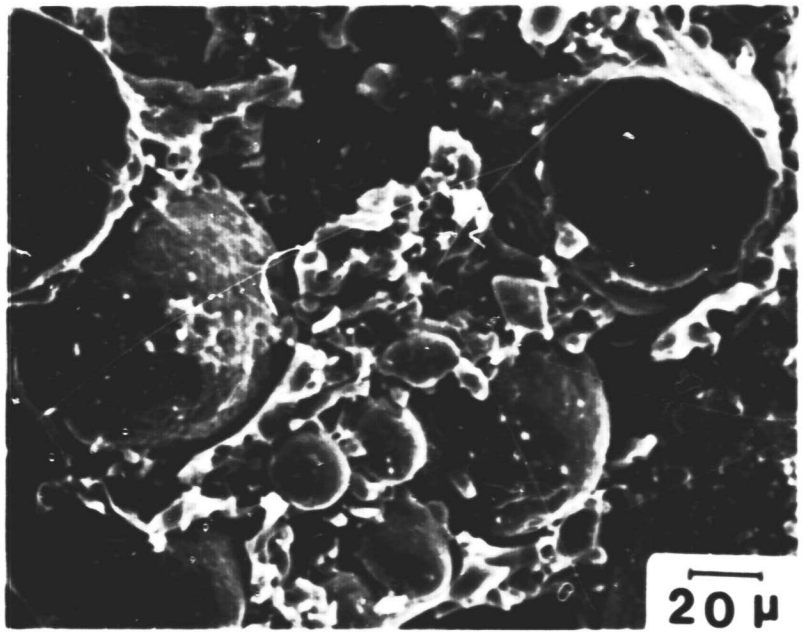

B

A fracture surface in Fig. 19 A is shown in Fig. 19 C. A broad particle size distribution of filler particles is seen here.

Two SEM photomicrographs of the aluminum powder No. 101 used as a filler in the L13 matrix are shown in Figure 20. The ellipsoidal particles cover a wide size distribution range. The ESCA analysis of the aluminum powder is given in Table IX.

The ESCA results are listed in Table XV. Runs No. 15 and No. 18 are different punches from the same sample. The sample for Run #13 showed more Al filler on the surface than the Run #15 sample. No Ti signal is observed consistent with cohesive failure. The Al signal here is consistent with the high density of filler particles (Fig. 19 C). The Si signal here could arise from the scrim cloth visible in Fig. 18 B.

3. L13-phosphate/fluoride-room temperature [L13-D-5, RT] - This sample failed interfacially. The adhesive popped off when that lap shear member was punched. The metal failure surface shows islands of polymers left behind as in the [L13-A-2, RT] case. The adhesive substrate surface mirrors the metal substrate surface as was noted in the [PPQ-D-5, RT] sample. The EDAX spectrum of the adhesive substrate surface showed Al and Ti signals.

The ESCA results are listed in Table XV. The adhesive failure surface shows a small Ti signal suggesting transfer of oxide layer from the adherend to the adhesive. A shake-up satellite for C 1s was observed at 291.0 ev which is a characteristic spectral feature of L13. The photopeak at 538.3 ev was assigned to an O 1s shake-up satellite which is unusual.

4. L13-phosphate/fluoride - 450° [L13-D-6, 450] - The failure mode here was mixed although this particular sample had a zero lap shear strength. The adhesive did not separate when the sample was punched. The SEM photomicrographs show no glass fibers but rather islands of adhesive on the

Figure 20.

SEM photomicrographs of No. 101 aluminum powder at 100X (A) and at 500 X (B).

Figure 20. SEM photomicrographs of No. 101 aluminum powder at 100X (A) and at 500X (B).

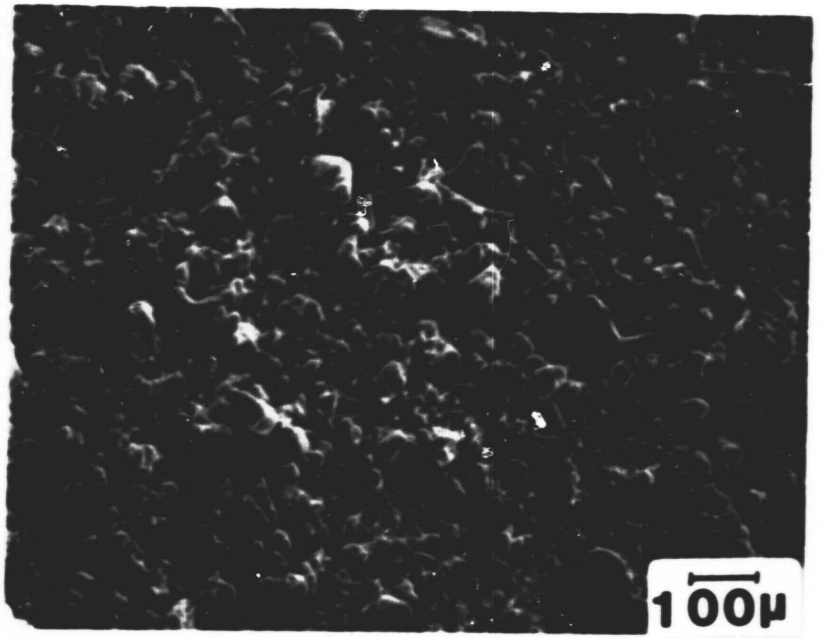

A

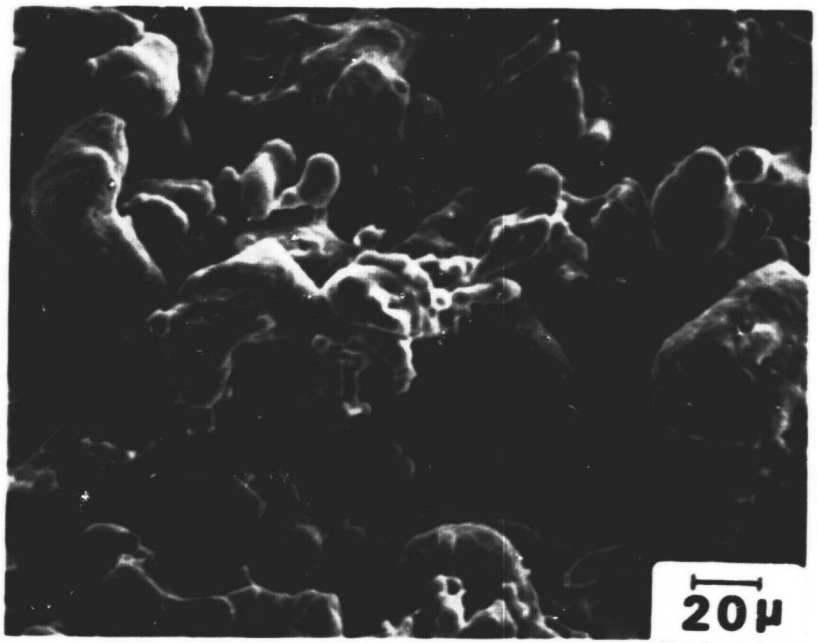

B

adherend surface as was seen in Fig. 17. The adherend surface shows features characteristic of phosphate/fluoride pretreatment (Fig. 10 A). The ESCA results are shown in Table XV. The Ti signal again reflects partial interfacial failure and the Ca signal was observed in the original phosphate/fluoride pretreated Ti 6-4.

F. Fractured Lap Shear Samples - L13 Mod I

1. L13 Mod I - chromic acid anodize - room temperature [L13 M1-A-9, RT] - This sample showed mixed mode failure. Examination of SEM photomicrographs showed that the fibers remain well wetted and intact with Al particles visible in and on the scrim cloth. The exposed adherend appeared to be covered with primer/adhesive. The ESCA results of this sample are shown in Table XVI. The weak Ti signal supports partial interfacial failure. However, the inability to scan the sample surface with ESCA necessarily means one cannot differentiate between exposed adherend surface or a collection of debris produced on fracture on the adhesive-containing areas.

2. L13 Mod I - chromic acid anodize - 450° [L13 M1-A-6, 450] - The sample showed mixed mode failure and the SEM photomicrographs here are quite similar to the room temperature sample [L13 M1-A-9, RT] discussed above. The ESCA results are shown in Table XVI. The Al signal is due to filler particles but an expected Ti signal was not observed. The fact that no Ti signal was observed could be due to sample bias.

3. L13 Mod I - phosphate/fluoride - room temperature [L13 M1-D-9, RT] - A mixed mode failure is observed here and the SEM photomicrographs show features characteristic of a phosphate/fluoride treated Ti 6-4 adherend (see Fig. 10 A). The ESCA results in Table XVI support again partial interfacial failure by observation of the Ti signal.

4. L13 Mod I - phosphate/fluoride - 450° [L13 M1-D-6, 450] - Interfacial failure was noted in this sample and the SEM photomicrographs of the adherend

TABLE XVI

ESCA RESULTS OF FRACTURED LAP SHEAR [L13M1] SAMPLES

Sample	Photopeak	B.E.(ev)	A.F.
[L13M1-A-9, RT]	O 1s	532.2	0.16
	Ti $2p_{3/2}$	458.8	0.0065
	N 1s	400.2	0.045
	C 1s	(285.0)	0.79
[L13M1-A-6, 450]	O 1s	531.9	0.17
	N 1s	399.9	0.043
	C 1s	(285.0)	0.75
	Al 2s	119.1	0.035
[L13M1-D-9, RT]	O 1s	532.6	0.23
	Ti $2p_{3/2}$	458.8	0.037
	N 1s	400.3	0.044
	C 1s	(285.0)	0.69
[L13M1-D-6, 450]	O 1s	531.6	0.23
	Ti $2p_{3/2}$	458.6	0.031
	N 1s	400.2	0.047
	C 1s	(285.0)	0.69

surface appeared similar to Fig. 10 A. The SEM photomicrographs in Figure 21 show a high density of filler particles contained in the adhesive. There are several 'pockets' where Al particles have been displaced. The ESCA results in Table XVI are similar to what was seen for Sample [L13 M1-D-9, RT] above.

G. Fractured Lap Shear Samples - L13 Mod II

Only the 450° test samples were received on this series.

1. L13 Mod II - chromic acid anodize - 450° [L13 M2-A-2, 450] - The failure mode was interfacial in this case. The SEM photomicrographs show a thin layer of adhesive over the adherend with some thicker adhesive islands. The adhesive failure surfaces shows considerable deformation. The Al filler particles are seen but no scrim cloth is apparent. The ESCA results are shown in Table XVII. The metal failure surface shows Ti as evidence of interfacial failure and Si of undetermined origin. The adhesive failure surface shows Ti and suggests transfer of Ti from the adherend to the adhesive.

2. L13 Mod II - phosphate/fluoride-450° [L13 M2-D-8, 450] - Interfacial failure was observed for this sample. The adhesive popped off when punched. The SEM photomicrographs show a characteristic phosphate/fluoride pretreatment morphology for the metal failure surface. Scattered patches of primer/adhesive are also noted on the adherend. The metal substrate surface appears similar to the metal failure surface. The adhesive failure surface shows no scrim cloth but unbonded Al filler particles are seen. There are some voids and some deformation.

The ESCA results are listed in Table XVII. Ti is noted with the two metal surfaces but not on the adhesive failure surface suggesting that no surface oxide was transferred from the adherend to the adhesive on fracture. Ca noted on both metal surfaces and P noted on the metal substrate surface

Figure 21.

SEM photomicrographs of [L13M1-D-6, 450] at 1,000X (A) and at 5,000X (B).

Figure 21. SEM photomicrographs of [L13M1-D-6, 450] at 1,000X (A) and at 5,000X (B).

TABLE XVII

ESCA RESULTS OF FRACTURED LAP SHEAR [L13M2] SAMPLES

Sample	Photopeak	B.E.(ev)	A.F.
[L13M2-A-2, 450] Metal Failure Surface	O 1s	532.1	0.17
	Ti $2p_{3/2}$	458.7	0.011
	N 1s	400.3	0.039
	C 1s	(285.0)	0.77
	Si 2s	153.5	0.010
[L13M2-A-2, 450] Adhesive Failure Surface	O 1s	531.8	0.17
	Ti $2p_{3/2}$	458.8	0.0062
	N 1s	400.2	0.049
	C 1s	(285.0)	0.77
[L13M2-D-8, 450] Metal Failure Surface	O 1s	531.8	0.29
	Ti $2p_{3/2}$	458.4	0.038
	N 1s	399.1	0.024
	Ca $2p_{3/2}$	347.4	0.0045
	C 1s	(285.0)	0.65
[L13M2-D-8, 450] Adhesive Failure Surface	O 1s	532.0	0.17
	N 1s	400.2	0.040
	C 1s	(285.0)	0.79
[L13M2-D-8, 450] Metal Substrate Surface	O 1s	531.7	0.24
	Ti $2p_{3/2}$	458.6	0.047
	N 1s	400.2	0.031
	Ca $2p_{3/2}$	347.2	0.0047
	C 1s	(285.0)	0.66
	P 2s	191.3	0.0063
	Al 2s	119.3	0.012

are residuals left from the pretreatment (see Table VI).

H. Summary

A summary of the results obtained for the fractured lap shear samples are shown in Tables XVIII and XIX for the PPQ and L13 adhesives, resp. The following conclusions are based on the summary tables:

(1) There is a pronounced tendency for both adhesives to "pop-off" of the phosphate/fluoride pretreated surfaces independent of test temperature.

(2) The presence of Ti as established by ESCA can be used as a criteria for interfacial failure and as a criteria for fracture of the metal oxide layer.

(3) The presence of Pb in the surface of only the PPQ samples is not explained.

(4) The presence of Ca in both the PPQ and L13 samples is associated only with the Ti 6-4 adherend surfaces.

(5) The persistent observation of Si particularly in the PPQ samples needs to be rationalized. There are at least three sources of silica in the adhesive system, namely (i) scrim cloth, (ii) degradation of scrim cloth coating and (iii) contamination of neat polymer.

I. Titania Powders

BET surface areas determined by N_2 adsorption and the crystalline phases determined by x-ray diffraction for the 4 titania powders A1, A2, R1, and R2 are given in Table V. Calculated d spacings of 0.325 nm for rutile and 0.352 nm for anatase agree well with reported values (18). The elemental composition of the titania powders by ESCA analysis is given in Table XX. Powder A2 appears to be pure without any trace elements. Aluminum (III) is present on both rutile samples presumably as a thin (<5 nm)

TABLE XVIII

SUMMARY RESULTS FOR FRACTURED LAP SHEAR PPQ SAMPLES

							ESCA								
ADH	PT	T	LSS	FM	AS	SA	Al	Ca	F	P	Pb	Si	Ti	V	Sample No.
-	A	-	-	-	-	-			X				X		
-	D	-	-	-	-	-		X	X	X			X		
PPQ	A	RT	4650	C	No	-						X			PPQ-A-7, RT
PPQ	A	450°	2820	C	No	-		X				X			PPQ-A-2, 450
PPQ	D	RT	1950	I	Yes	MFS		X				X	X		PPQ-D-5, RT
						AFS						X			
						MSS		X			X		X	X	
						ASS					X		X		
PPQ	D	450°	3000	C	Yes	AFS		X				X			PPQ-D-4, 450
						MSS		X			X		X	X	
						ASS					X		X		
PPQM1	A	RT	2290	I-C	No	-		X			X	X	X		PPQM1-A-7, RT
PPQM1	A	450°	972	I-C	No	-									PPQM1-A-4, 450
PPQM1	D	RT	720	I	Yes	MFS		X	X		X	X	X		PPQM1-D-5, RT
						AFS						X	X		
						MSS		X			X		X		
						ASS						X	X		
PPQM1	D	450°	1010	I-C	Yes	AFS						X			PPQM1-D-8, 450
						MSS		X			X		X		

ADH - Adhesive
PT - Pretreatment
T - Test temperature

LSS - Lap shear strength (psi)
FM - Failure mode
AS - Adhesive separation when punched

SA - Surface Analyzed
MFS - metal failure surface
AFS - adhesive failure surface
MSS - metal substrate surface
ASS - adhesive substrate surface

TABLE XIX

SUMMARY RESULTS FOR FRACTURED LAP SHEAR L13 SAMPLES

							ESCA								
ADH	PT	T	LSS	FM	AS	SA	Al	Ca	F	P	Pb	Si	Ti	V	Sample No.
L13	A	RT	2170	I-C	No	-						X	X	X	L13-A-2-RT
L13	A	450°	2168	C	No	-	X					X			L13-A-2, 450
L13	D	RT	870	I	Yes	MSS							X		L13-D-5,RT
						ASS							X		
L13	D	450°	0	I-C	No	-		X					X		L13-D-6, 450
L13M1	A	RT	2750	I-C	No	-							X		L13M1-A-9, RT
L13M1	A	450°	1940	I-C	No	-	X								L13M1-A-6, 450
L13M1	D	RT	1260	I-C	No	-							X		L13M1-D-9, RT
L13M1	D	450°	808	I-C	No	-							X		L13M1-D-6, 450
L13M2	A	450°	410	I-C	No	MFS						X	X		L13M2-A-2, 450
						AFS							X		
L13M2	D	450°	440	I	Yes	MFS		X					X		L13M2-D-8, 450
						AFS									
						MSS	X	X		X			X		

ADH - Adhesive
PT - Pretreatment
T - Test temperature

LSS Lap shear strength (psi)
FM - Failure mode
AS - Adhesive separation when punched

SA - Surface analyzed
MFS - metal failure surface
AFS - adhesive failure surface
MSS - metal substrate surface
ASS - adhesive substrate surface

TABLE XX

ESCA ANALYSIS OF TITANIA POWDERS

	Anatase-A1		Rutile-R1		Anatase-A2		Rutile-R2	
Photopeak	B.E.(ev)	A.F.	B.E.(ev)	A.F.	B.E.(ev)	A.F.	B.E.(ev)	A.F.
C 1s	(285.0)	0.22	(285.0)	0.33	(285.0)	0.42	(285.0)	0.36
O 1s			529.6				529.6	
	529.4	0.50	531.8	0.48	529.6	0.42	531.4	0.43
Ti $2p_{3/2}$	458.2	0.15	458.0	0.11	458.4	0.16	458.4	0.09
Al 2s	-	-	118.8	0.07	-	-	119.2	0.11
K $2p_{3/2}$	292.6	0.08	-	-	-	-	-	-
Cl 2p	198.0	0.01	197.8	0.004	-	-	-	-
P $2p_{3/2}$	132.8	0.03	-	-	-	-	-	-

alumina coating since a significant Ti signal is also observed. The oxygen photopeak on both rutile surfaces was a doublet. The peak at 529.2 ev is due to titanium oxide while the peak at 531.2 ev is due to aluminum oxide (19). SEM photomicrographs showed fine particles lumped together in all four powders.

The heats of immersion ($\Delta_w H$) values of the titania powders in water as a function of the outgassing temperature of the powder are shown in Figure 22. The $\Delta_w H$ values for the anatase -A1 powder do not change as much with outgassing temperature, as the R1, R2 and A2 samples. A similar behavior has been shown previously by Herrington and Lui (20) and Iwaki et al. (21). For rutile-R1, $\Delta_w H$ increases rapidly up to 300°C and less rapidly to 400°C. Anatase A2 which is a mixture of rutile and anatase shows $\Delta_w H$ values between rutile and anatase.

Water adsorption isotherms for A1, A2, and R1 samples as a function of outgassing temperature are shown in Figures 23, 24 and 25 respectively. The water adsorption data are consistent with the heat of immersion data. The rutile R1 shows an increase in water adsorption with increasing outgassing temperature up to 300°C, while water adsorption on anatase does not show a significant dependence on outgassing temperature. Water adsorption on A2 shows an intermediate behavior of rutile and anatase, with outgassing temperature. Day (22), Jones and Hockey (23) and Dawson (24) have all shown that the following three types of H_2O may exist on a TiO_2 surface: (i) dissociatively chemisorbed water present as hydroxyl groups; (ii) non-dissociatively chemisorbed water found as a co-ordinating ligand to surface cation Lewis acid sites; and, (iii) physically adsorbed water present in a monolayer and in multilayers. Jones and Hockey (23) and Day (22) have shown that non-dissociative chemisorbed molecular water on the (100) and (101) planes of

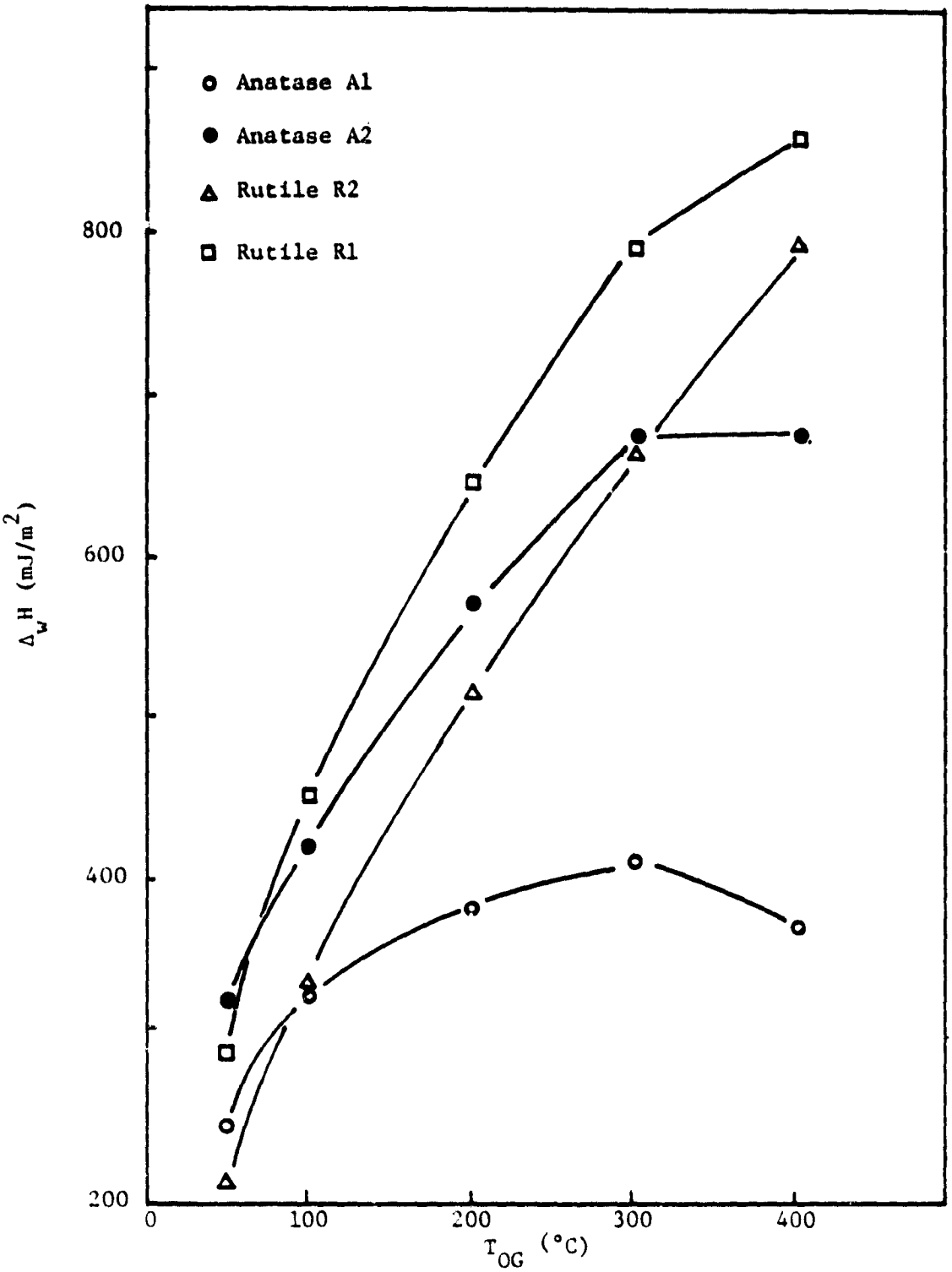

Figure 22. Heats of immersion ($\Delta_w H$) of TiO_2 powders in water as a function of outgassing temperature (T_{OG}).

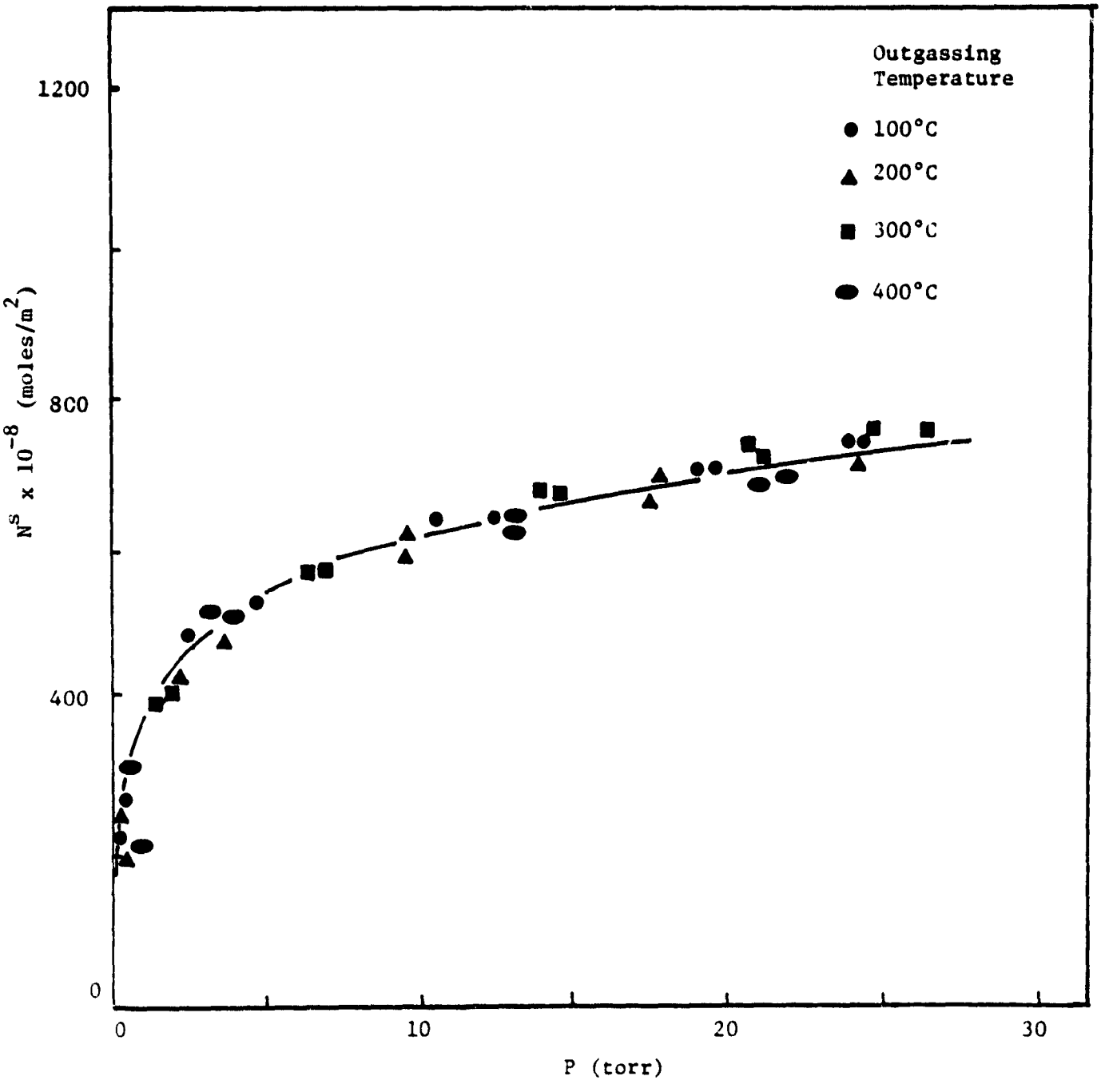

Figure 23. Adsorption isotherm at 30°C for water on anatase Al.

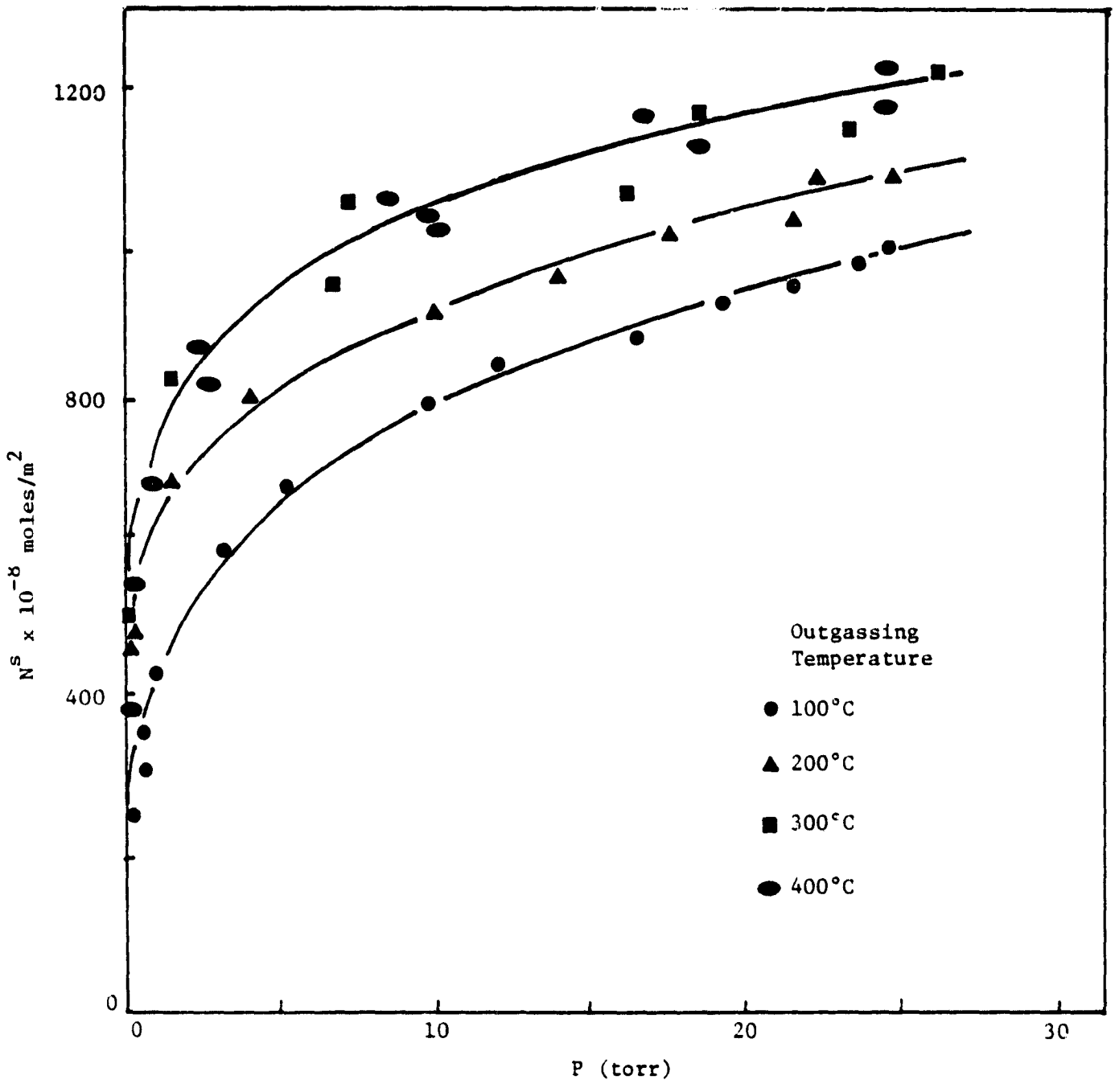

Figure 24. Adsorption isotherm at 30°C for water on anatase A2.

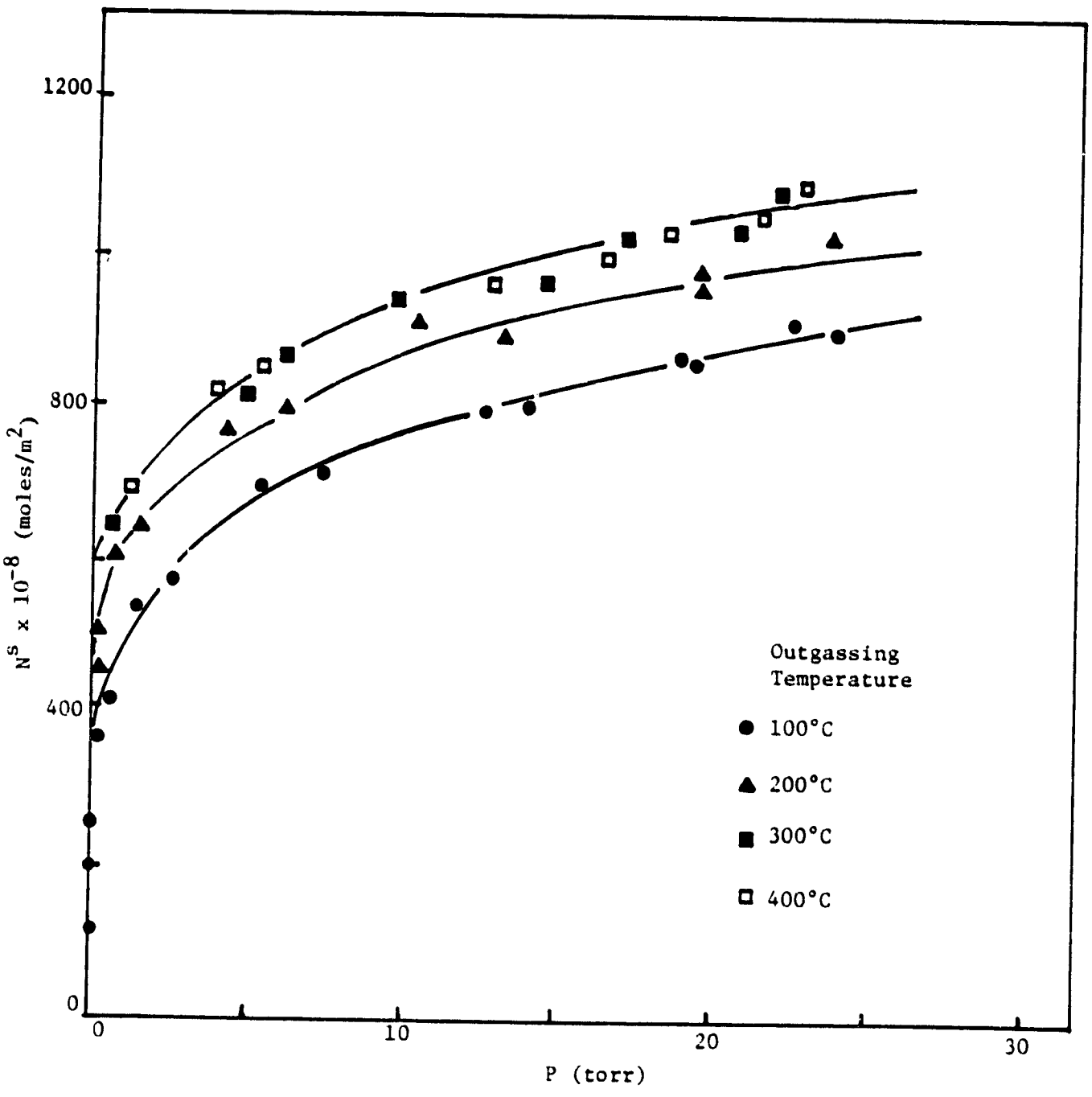

Figure 25. Adsorption isotherm at 30°C for water on rutile R1.

TiO_2 is retained up to 200°C and hydroxyl groups which arise from dissociative chemisorption on the (110) plane are nearly all desorbed on outgassing at 400°C. Thus the increase in water adsorptive capacity of rutile with increasing temperature can be explained in terms of successive desorption of different kinds of hydroxyl groups present on the surface. Rehydroxylation of the evacuated TiO_2 surfaces occurs when the surface is again exposed to water. Anatase does not show any variation in water adsorption capacity with outgassing temperature. Dawber et al. (25) have shown that rutile adsorbed more water than anatase per unit area and also that dried anatase re-adsorbed approximately only one molecular water layer whereas dried rutile could re-adsorb about 6 molecular water layers. Thus the decreased water adsorptive capacity of anatase with increased outgassing temperature is in agreement with the work by Dawber et al. (25).

Acidity measurements taken with indicators are given in Table XXI. All four powders were found to be basic and their pKa values < 7.6. When the powders were evacuated at 400°C for 2 hours an increase in acid strength was observed on rutile-R1, with a measured pKa value between 7.0 and 7.6. The increase in acid strength may be due to the exposure of coordinately unsaturated cations by removal of water molecules at a higher temperature (26).

The isoelectric points (i.e.p.) measured with microelectrophoresis for R1, R2, A1 and A2 samples are 5.1, 6.6, 3.8, and 5.6 respectively. The presence of Cl on both the A1 and R1 samples was seen by ESCA in Table XX. However the anatase-A1 sample has a larger amount of Cl compared to the rutile-R1 sample. Parfitt et al. (13) have suggested that the surface chlorine plays an important role in determining the isoelectric point in TiO_2 powders. He indicated that both surface and bulk chloride have the

TABLE XXI

ACIDITY MEASUREMENTS ON TITANIA POWDERS

Indicator	pK_a	Color of base form	Color of acid form	Evacuated at room temp.				Evacuated at 400°C			
				A1	R1	R2	A2	A1	R1	R2	A2
p-nitrophenol	7.6	Y	C	C→Y	C→Y	C→Y	C→Y	C→Y	C→C	C→Y	C→Y
o-nitrophenol	7.0	Y	C	Y→Y	Y→Y	Y→Y	Y→Y	Y→Y	Y→Y	Y→Y	Y→Y
alizarin	6.8	R	Y	Y→R	Y→R	Y→R	Y→R	Y→R	Y→R	Y→R	Y→R

C - colorless

Y - yellow

R - red

effect of lowering the i.e.p. Thus our results are consistent with his findings. Anatase-A1 has the lowest i.e.p. and rutile-R1 has a lower i.e.p. than the other two powders. When the pH was adjusted with HCl and NaOH instead of HNO_3 and KOH, no change in the i.e.p. was observed. Even though the surface chloride ions changes the i.e.p. value, the external addition of chloride ions does not change the i.e.p.

Solutions of 5% PPQ [1:1 xylene : m-cresol], and 22% LaRC-13 [dimethylformamide] are used as primers on freshly pretreated Ti 6-4 metal coupons. The heat of immersion values of the TiO_2 powders in these solutions are listed in Table XXII. The $\Delta_w H$ values in 1:1 xylene : m-cresol are similar for all four powders. However, the heat of immersion for anatase A1 is higher in the 5% PPQ solution than that in the solvent o-ly. For the other three powders, the $\Delta_w H$ values are similar in the solvent and in the 5% PPQ solution. Thus there appears to be a specific, preferential interaction of PPQ with anatase A1. This may be due to the lower water adsorption capacity and the higher chloride content on the anatase A1 surface compared to other powders as seen by the water adsorption and ESCA studies. Surface hydroxyl groups, cations, and chloride groups on anatase A1 are not covered with water molecules and are readily available for interaction with PPQ. The $\Delta_w H$ values for anatase A1 on immersion in PPQ solutions of different concentrations are shown in Figure 26. The $\Delta_w H$ values increase with increasing concentration of the polymer. This further confirms that there is specific kind of interaction with the polymer on the anatase A1 surface.

The $\Delta_w H$ values in Table XXII for DMF and for 22% LARC-13 are similar for each of the TiO_2 powders. This means there apparently is no preferential interaction of the LARC-13 polymer with any of the TiO_2 powders.

TABLE XXII

HEATS OF IMMERSION OF TITANIA POWDERS IN XYLENE:m-CRESOL, 5% PPQ, DIMETHYLFORMAMIDE(DMF) AND 22% LARC-13

	$\Delta_w H(mJ/m^2)$			
Liquid	A	R1	R2	A2
1:1 xylene : m-cresol	252	282	229	273
5% PPQ in 1:1 xylene : m-cresol	382	271	274	286
DMF	267	326	240	342
22% LARC-13 in DMF	279	320	227	362

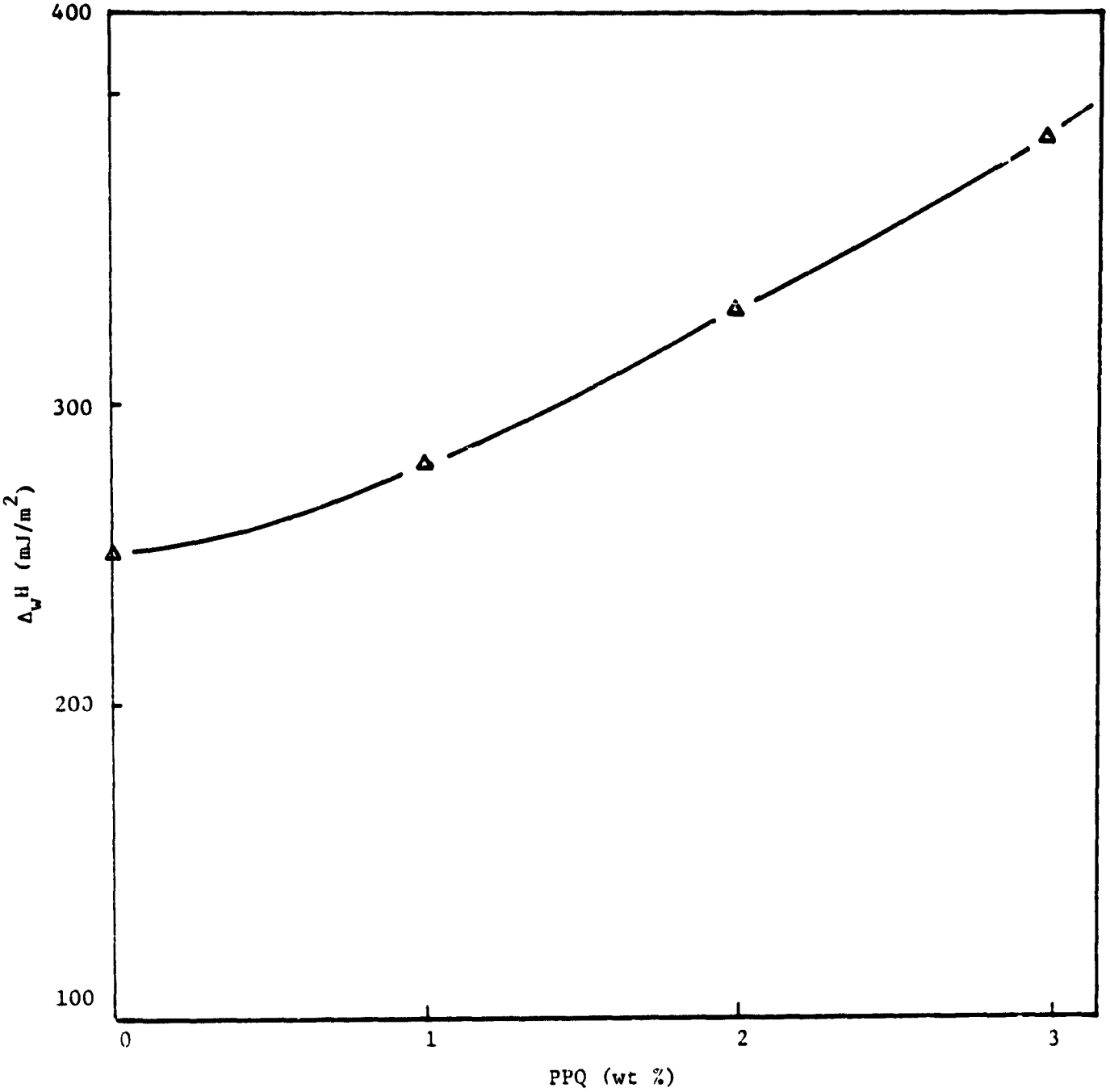

Figure 26. Heats of immersion ($\Delta_w H$) of anatase Al into PPQ/xylene: m-cresol solutions as a function of PPQ concentration.

IV. REFERENCES

(1) L. Taylor, Ed., "Metals Handbook, Atlas of Microstructure of Industrial Alloys," Vol. 7, p. 321, Am. Soc. Metals, Metals Park, OH (1972).

(2) W. C. Hamilton, Appl. Polym. Symp., No. 19, 105 (1972).

(3) T. Smith and D. H. Kaelble, "Mechanism of Adhesion Failure Between Polymers and Metallic Substrates: Al 2024-T3 and Ti 6-4 with HT 424 Adhesive," Report No. 74-73, Air Force Materials Labr., Wright-Patterson AFB, OH (1974).

(4) R. F. Wegman and J. Bodner, SAMPE Quart. 5(1), 28 (1973).

(5) A. Benninghoven et al., Appl. Phys. Lett., 31, 341 (1977).

(6) K. W. Allen and H. S. Alsalim, J. Adhes., 6, 229 (1974).

(7) F. Motte et al., Oxid. Met., 10, 113 (1976).

(8) F. Dalard et al., Surf. Technol., 4, 367 (1976).

(9) H. D. Shih and F. Jona, Appl. Phys., 12, 311 (1977).

(10) R. F. Wegman, Appl. Polym. Symp., No. 19, 385 (1972).

(11) P. M. Stifel, New Ind. Appl. Advan. Mater. Technol., Nat. SAMPE Symp. Exhib., 19th, p. 73, SAMPE, Azusa, CA (1974).

(12) S. J. Gregg and K. S. W. Sing, "Adsorption, Surface Area and Porosity," Academic Press, New York (1967).

(13) G. D. Parfitt, J. Ramsbotham and C. H. Rochester, J. Colloid Interf. Sci. 41, 437 (1972).

(14) J. G. Mason, R. Siriwardane and J. P. Wightman, J. Adhesion, in press.

(15) J. H. Scofield, J. Electron Spectroscopy and Related Phenomena, 8, 129 (1976).

(16) A. B. Desai and G. L. Wilkes, J. Polymer Sci., Symposium No. 46, 291 (1974).

(17) Y. Kang, M. S. Thesis, VPI & SU, Blacksburg, VA, 1978.

(18) "Select Powder Diffraction Data for Minerals" 2, 1974, Joint Comm. on Powder Diffraction Standards, 49.

(19) R. R. Bailey and J. P. Wightman, J. Colloid Interf. Sci., 70, 112, (1979).

(20) K. D. Herrington and Y. K. Lui, J. Colloid Interf. Sci., 34, 447 (1970).

(21) T. Iwaki, M. Komuro and M. Miura, Bull. Chem. Soc. Japan, 45, 2343 (1972).

(22) R. E. Dessy, Progr. Organic Coatings, 2, 269 (1973/4)

(23) P. Jones and J. A. Hockey, J. Chem. Soc. Faraday Trans I, 68, 907 (1972).

(24) T. T. Dawson, J. Phys. Chem., 71, 838 (1967).

(25) J. G. Dawber, L. B. Guest and I. Lambourne, Thermochimica Acta, 6, 411 (1973).

(26) G. D. Parfitt, D. Urwin and T. J. Wiseman, J. Colloid Interf. Sci., 36, 217 (1971).

(27) C. L. Hendricks, "Evaluation of High Temperature Structural Adhesives for Extended Service", NASA Contract NAS1-15605 Semi-Annual Report, Boeing Aerospace Co., June 1979.

V. ACKNOWLEDGEMENT

The expertise of Mr. Bob Honeycutt in the operation of the scanning electron microscope is acknowledged.

APPENDIX I

ADHEREND SURFACE TREATMENT PROCESSES (27)

A brief description of each surface treatment is provided in this portion of the Appendix.

A. Chromic Acid Anodize

The process procedures used for this surface treatment are found in Boeing specification BAC 5980. These procedures included:

(1) Alkaline clean (Turco 2623) 15 minutes @ 333K (140°F)
(2) Hot rinse
(3) Nitric - hydrofluoric etch 90 seconds at 294K (70°F)
(4) Cold rinse
(5) CrO_3 Anodize - 5 volts, 12.7 Amps/M^2 (1.2 Amps/FT^2)
    - CrO_3 48.8 gm/Liter (6.5oz./gallon)
    - 20 minutes @ 291K (65°F)
(6) Cold rinse
(7) Hot air dry @ 338K (150°F)

B. Phosphoric Acid Anodize

The process procedures for this surface treatment are as specified in Boeing specification BAC 5555. General procedures are:

(1) Alkaline clean (Turco 2623) 15 minutes @ 333K (140°F)
(2) Hot rinse
(3) Nitric - hydrofluoric etch 90 seconds @ 294K (70°F)
(4) Cold rinse
(5) Phosphoric acid anodize - 5 volts, 19 Amps/M^2 (1.8 Amps/FT^2)
    - H_3PO_4 - 112.5 gm/liter (15 oz/gallon)
    - 20 minutes @ 297K (75°F)
(6) Cold rinse
(7) Hot air dry @ 338K (150°F)

C. Pasa-Jell 107

These process procedures for this treatment are:

(1) Alkaline clean (Turco 2623) 15 minutes @ 333K (140°F)
(2) Hot rinse
(3) Nitric-hydrofluoric etch 90 seconds @ 294K (70°F)
(4) Pasa-Jell 107 12 minute immersion in Pasa-Jell 107
(5) Hot air dry @ 338K (150°F)

D. Phosphate Fluoride (Boeing)

Process procedures for this surface treatment are as specified in Boeing specification BAC 5514. General procedures are:

(1) Alkaline clean (Turco 2623) 15 minutes @ 333K (140°F)
(2) Hot rinse
(3) Nitric - hydrofluoric etch 90 seconds @ 294K (70°F)
(4) Cold rinse
(5) Phosphate fluoride treat per BAC 5514 105 seconds @ 294K (70°F)
(6) Cold rinse
(7) Hot water leach 15 minutes @ 355K (180°F)
(8) Hot air dry @ 338K (150°F)

E. Phosphate Fluoride (Picatinny)

General procedures for this surface treatment are:

(1) Alkaline clean (Turco 2623) 15 minutes @ 333K (140°F)
(2) Hot rinse
(3) Nitric-hydrofluoric etch, BAC 5514 Method II with 7.5 g/liter (28.4 oz/gallon) anhydrous sodium sulfate added, 90 seconds @ 294K (70°F)
(4) Cold rinse
(5) Phosphate Fluoride per BAC 5514, 105 seconds @ 294K (70°F)
(6) Cold rinse
(7) Hot water leach 15 minutes @ 355K (180°F)
(8) Hot air dry @ 339K (150°F)

F. Phosphate Fluoride with grit blast

This procedure is identical to process D. above except for the grit blast. The general process is:

(1) Vacuum blast with 80 grit aluminum oxide @ 0.21 MPa (30 psi)
(2) Alkaline clean (Turco 2623) 15 minutes @ 333K (140°F)
(3) Hot rinse
(4) Nitric-hydrofluoric etch 90 seconds @ 294K (70°F)
(5) Cold rinse
(6) Phosphate fluoride treat per BAC 5514 105 seconds @ 294K (70°F)
(7) Hot water leach @ 355K (180°F)
(8) Hot air dry @ 338K (150°F)

G. Turco 5578

General procedure for this process are:

(1) Alkaline clean (Turco 2623) 15 minutes @ 333K (140°F)
(2) Hot rinse
(3) Turco 5578 immersion, 10 minutes @ 361K (190°F)
solution = 432 gms/liter (3.6 LB/gallon)
(4) Hot rinse
(5) Hot air dry @ 338K (150°F)

H. RAE Process ($NaOH/H_2O_2$)

General procedures for this British developed process are:

(1) Vacuum blast with 90 grit aluminum oxide @ 0.21 MPa (30 psi)
(2) Alkaline clean (Turco 2623) 15 minutes @ 333K (140°F)
(3) Hot rinse
(4) Immerse in solution of 20 g/liter (76 oz/gallon) sodium hydroxide plus 30% hydrogen peroxide 22.5 ml/liter
(3 oz/gallon) added immediately prior to immersion
(5) Hot rinse
(6) Hot air dry @ 338K (150°F)

Common solutions for the above surface treatments using BAC 5514 are:

(1) Turco 2623 alkaline cleaner
Concentration: 37.5 - 60 gm/liter (5-8 oz/gallon)
operating temperature: 330 - 352K (135-175°F)
(2) Nitric - hydrofluoric etch solution
- Nitric Acid (40-42 DEG BE) = 300 - 450 gm/liter (40-60 oz/gallon)
- Hydrofluoric acid (70%) - sufficient to maintain etch rate
- FC -95 wetting agent - surface tension of 35-45 dynes/cm
- Operating temperature = 291-305K (65-90°F)
- Etch rate 0.008 - 0.020 mm (0.002-0.005 inch)/surface/hour
(3) Phosphate fluoride solution
- Sodium phosphate ($Na_3PO_4 \cdot 12H_2O$), 45-50 gm/liter (6.3-6.7 oz/gal.)
- Potassium fluoride ($KF \cdot 2H_2O$), 19-30 gm/liter (2.5-4.0 oz/gal.)
- Hydrofluoric acid (HF), 15-21 gm/liter (2.0-2.8 oz/gal.)
- Operating temperature = ambient

APPENDIX II

CANDIDATE ADHESIVE RESINS (27)

1) LARC-13 Polyimide Adhesive - This resin was selected as an adhesive candidate based on preliminary data obtained by Boeing which demonstrated good elevated temperature thermal stability and desireable failure modes. The base resin synthesis and cure chemical reactions are illustrated below:

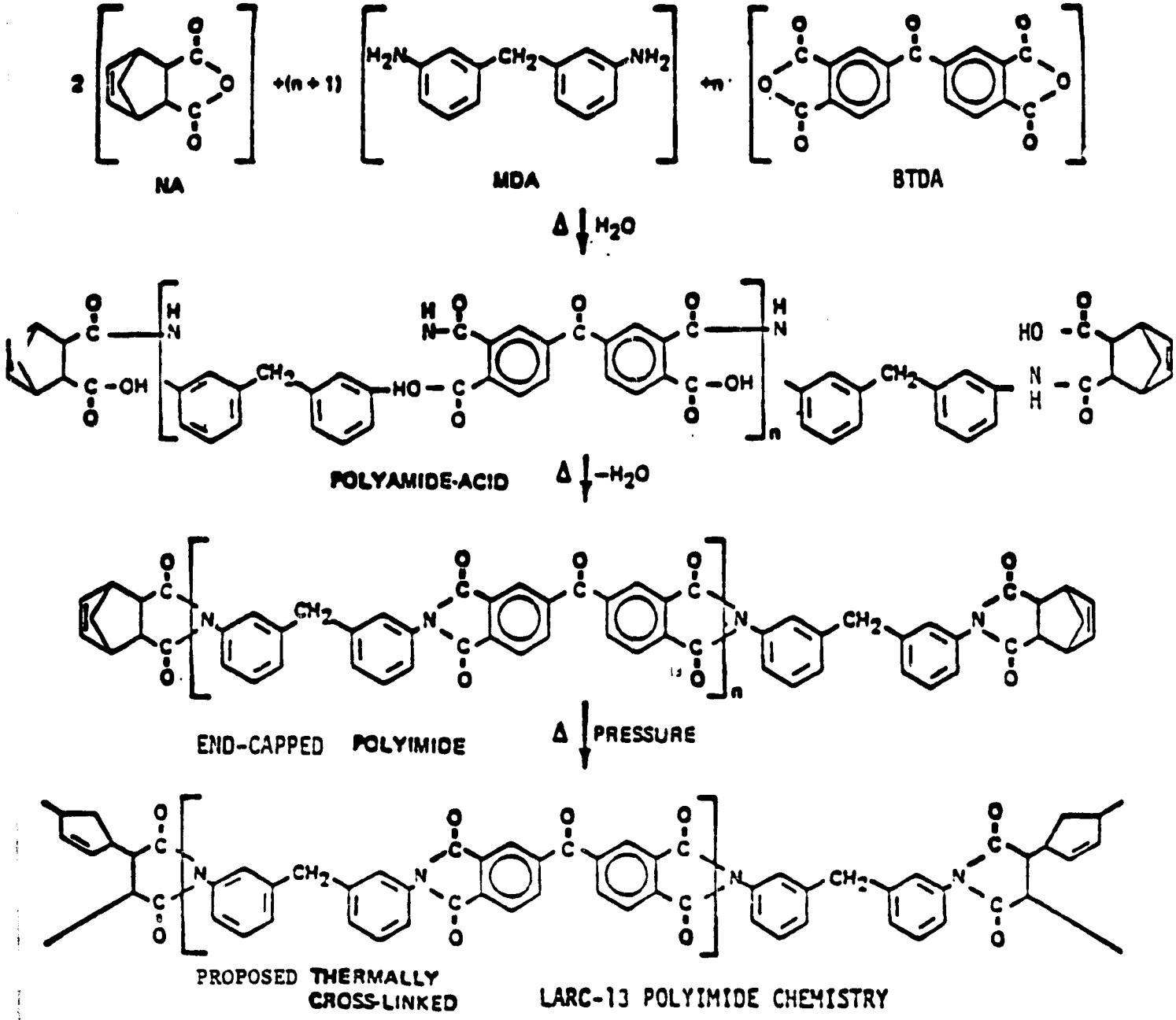

LARC-13 base resin formulated with 30 weight percent aluminum powder (Alcoa 101) is supplied by NASA Langley for this program. The adhesive is subsequently impregnated by Boeing on Style 112, A-1100 finish glass fabric and B-staged to a low flow state. The control of B-staging just prior to crosslinking reaction is critical to low or no volatile release during final cure.

2) LARC-13 Modification I LARC-13 does demonstrate good adhesive properties, however, it also exhibits undesirable processing characteristics. This modification consisted of Amoco Amide-imide AI-1130 mixed at 50 phr with the base LARC-13 formulation plus addition of Alcoa 101 aluminum powder to 60 phr. This adhesion formulation provides controlled flow and honeycomb filleting for structural bonding. Style 112, A-1100 glass fabric films were prepared for bonding operations.

3) LARC-13 Modification II In addition to copolymer (amide-imide) studies performed on Modification I, a second modification was selected/evaluated which involves methyl nadic capped polymer and addition of 20 mole percent of meta phenylene diamine as codiamines. This results in a nominal polymer molecular weight of 1,300. The modification procedures just described were performed by Boeing technical personnel using identical synthesis procedures as those used by NASA Langley RC in making the LARC-13 resin.

4) Polyphenylquinoxaline (PPQ) This resin is supplied by NASA Langley as monoether polyphenylquinoxaline in a solvent mixture 1:1 of practical grade m-Cresol and mixed xylenes. Solids content is reported at 16.6% based upon final polymer weight. PPQ has demonstrated excellent elevated temperature stability and represents a different family of polymers for evaluation in this program.

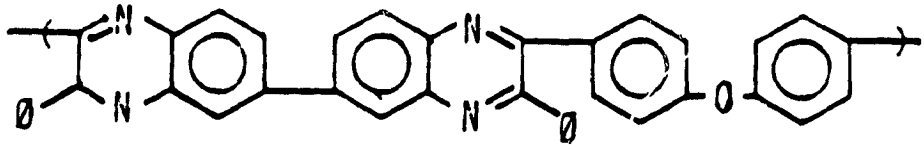

5) PPQ MOD I This modification consists of the addition of boron powder at 30 phr. This modification was done in an attempt to modify the adhesive's coefficient of thermal expansion to the coefficient of thermal of expansion of the metal substrate. This modification was deemed desirable for adapting the system for large area bonding.

APPENDIX III

NASA-LANGLEY POLYMER WORK

Experimental work was conducted at the NASA Langley Research Center polymer laboratory on the synthesis, characterization, and evaluation of the following materials as high performance and/or high temperature adhesives and laminating resins.

1. **Acetylene-Terminated Imide Oligomers and Polymers Therefrom**

2. **Acetylene-Terminated Phenylquinoxaline Oligomers and Polymers Therefrom**

3. **Polyphenylquinoxalines**

4. **Cyanato-Terminated Polysulfones**

Work of a more basic nature was performed on the development of novel crosslinking routes and the elucidation of a unique hydration of an ethynyl substituted imide.

Consultation to NASA was provided in the following areas.

1. Improved structural resins for conventional use (rubber toughened epoxies and cyanates, polysulfones, and 250 and 350°F cure epoxies)

2. Quality control of epoxy graphite prepreg

3. High temperature adhesives for titanium joining

4. High temperature laminating resins

The following papers were presented or published during this reporting period. Abstracts are provided where appropriate.

1. "Thermal Reaction of Ethynyl Phthalimides and Hydration of N-(4-Ethynylphenyl)phthalimides" P. M. Hergenrother Journal of Heterocyclic Chemistry 17, 5 (1980).

Three ethynyl substituted phenylphthalimides were prepared and characterized by high pressure liquid chromatography, differential scanning calorimetry, and mass spectroscopy. When the preparation of N-(4-ethynylphenyl)phthalimide was attempted by the thermal cyclodehydration of N-(4-ethynylphenyl)-2-carboxybenzamide, N-(4-acetylphenyl)phthalimide was obtained as the major component. This unusual hydration of an ethynyl group was investigated and a mechanism was proposed to explain it.

2. "Acetylene-Terminated Imide Oligomers and Polymers Therefrom" 180th National American Chemical Society Meeting, 1980; P. M. Hergenrother Div. Polymer Chemistry Preprints 21(1), 81 (1980).

Acetylene-terminated imide oligomers (ATIs) prepared by end-capping anhydride-terminated amic acid oligomers with ethynyl substituted aromatic amines (e.g. 3-ethynylaniline) followed by cyclodehydration are being evaluated as high temperature structural resins. As part of this program, amine terminated amic acid oligomers were end-capped with 4-ethynylphthalic anhydride and subsequently cyclodehydrated to provide a new series of ATIs. These materials were characterized primarily by differential scanning calorimetry (DSC) and torsional braid analysis (TBA). The ATIs were thermally cured and the resultant polymers characterized by thermogravimetric analysis (TGA) and isothermogravimetric analysis (ITGA). Prior to polymer work, a model compound, N-phenyl-4-ethynylphthalimide was prepared and its thermally induced reaction compared with that of two other ethynyl substituted phenylphthalimides. In addition, work was conducted to show why the 4-ethynylphenyl terminated imide oligomers failed to process and cure like that of the 3-ethynylphenyl end-capped oligomers (e.g. Thermid-600$^{(R)}$). During the thermal cyclodehydration of 4-ethynylphenyl terminated amic acid oligomers, a substantial portion of the ethynyl groups undergo hydration to yield 4-acetylphenyl terminated imide oligomers.

3. "Acetylene-terminated Oligomers and Polymers Therefrom" Gordon Research Conference on Polymers, Santa Barbara, California, January 1980.

4. "Acetylene-Containing Precursor Polymers" P. M. Hergenrother Journal of Macromolecular Science-Reviews in Macromolecular Chemistry C19(1), 1 (1980).

The use of the ethynyl group as a means of thermally chain extending, rigidizing, and crosslinking high temperature and/or high performance polymers was reviewed. This included the synthesis, thermally induced reaction, nature of the product, and properties of ethynyl containing polymers.

5. "Status of High Temperature Laminating Resins and Adhesives" P. M. Hergenrother and N. J. Johnston in Resins for Aerospace (Clayton A, May, ed.) ACS Symposium Series 132, p. 3.

APPENDIX IV

LISTING OF PUBLICATIONS AND PRESENTATIONS (1974-1981)

Publications

1. Thurman A. Bush, Mary Ellen Counts and J. P. Wightman, "The Use of SEM, ESCA and Specular Reflectance IR in the Analysis of Fracture Surfaces in Several Polyimide/Titanium 6-4 Systems" in Adhesion Science and Technology, Part A, L.-H. Lee, Editor, pp. 365-394, Plenum Press, New York (1975).

2. David W. Dwight, Mary Ellen Counts and James P. Wightman, "Surface Analysis and Adhesive Bonding. II. Polyimides", in Colloid and Interface Science, Vol. III, M. Kerker, Ed., pp. 143-156, Academic Press, New York (1976).

3. David W. Dwight and J. P. Wightman, "Identification of Contaminants", J. Environmental Sciences, XXI, No. 6, 28-31 (1978).

4. David W. Dwight, James E. McGrath and James P. Wightman, "ESCA Analysi of Polymer Structure and Bonding ", J. Appld. Polymers Science: Appld. Polym. Symp., 34, 35-47 (1978).

5. David W. Dwight and James P. Wightman, "Identification of Contaminants with Energetic Beam Techniques" in Surface Contamination: Genesis, Detection and Control, Vol. 2, K. L. Mittal, Ed., pp 569-586, Plenum Press, New York (1979).

6. W. Chen, D. W. Dwight, W. R. Kiang and J. P. Wightman, "Reduction of Contamination on Titanium Surface Studied by ESCA" in Surface Contanination: Genesis, Detection and Control, Vol. 2, K. L. Mittal, Ed.. pp 655-667, Plenum Press, New York (1979).

7. Wen Chen, Ranjani Siriwardane and J. P. Wightman, "Spectroscopic Characterization of Titanium 6-4 Surfaces after Chemical Pretreatments." in Proc. 12th SAMPE Techn. Conf., M. Smith, Ed., pp 896-903. SAMPE, Azusa, CA (1980).

8. John G. Mason, Ranjani Siriwardane and James P. Wightman, "Spectroscopic Characterization of Acidity of Titanium (6%, Al - 4%, V) Surfaces", J. Adhesion, 11, 000 (1980).

Presentations

1. J. P. Wightman and T. A. Bush, "Interfacial Characterization of Adhesive Systems: Polyimide/Titanium Alloy", Am. Chem. Soc., 26th SE Reg. Meetg., Norfolk, VA., Oct., 1974.

2. J. P. Wightman and T. A. Bush and M. E. Counts, "The Use of Scanning Electron Microscopy, Electron Spectroscopy for Chemical Analysis (ESCA), and Specular Reflectance Infrared Spectroscopy in the Analysis of Several Polyimide/Titanium 6-4 Systems," Am. Chem. Soc., 169th Natl. Meetg., Philadelphia, PA, April, 1975.

3. J. P. Wightman, T. A. Bush and M. E. Counts, "Effect of Surface Properties on the Adhesion of Titanium Bands", 53rd Va. Acad. Sci. Meetg., Harrisonburg, VA, May, 1975.

4. D. W. Dwight, M. E. Counts and J. P. Wightman, "Surface Analysis and Adhesive Bonding. II. Polyimides", Intl. Conf Colloid and Surface Chem., San Juan, P.R., June, 1976.

5. D. W. Dwight, J. E. McGrath and J. P. Wightman, "ESCA Analysis of Polymer Structure and Bonding", Am. Chem. Soc., 175th Natl. Meetg., Chicago, Ill., Aug., 1977.

6. D. W. Dwight, J. E. McGrath and J. P. Wightman, "ESCA Analysis of Polymer Structure and Bonding", Am. Chem. Soc., 9th Central Reg. Meetg., Charleston, W. Va., Oct., 1977.

7. D. W. Dwight, W. Chen and J. P. Wightman, "Surface Analysis and Adhesive Bonding. III. Ti 6-4", 29th Pittsburgh Conf., Cleveland, OH, Feb., 1978.

8. J. P. Wightman and D. W. Dwight, "Identification of Contaminants", 4th Intl. Symp., Contamination Control, Washington, D.C., Sept., 1978.

9. J. P. Wightman, W. Chen, D. W. Dwight and W. R. Kiang, "An XPS Study of Quantitative Comparison of Techniques to Remove Carbon Contamination from Metal Surfaces", 4th Intl. Symp. Contamination Control, Washington, D.C., Sept., 1978.

10. R. Siriwardane and J. P. Wightman, "Spectroscopic Characterization of the Surface Acidity of Metals", 54th Colloid and Surface Science Symp., Bethlehem, PA, June, 1980.

11. J. P. Wightman, W. Chen and R. Siriwardane, "Spectroscopic Characterization of Ti 6-4 Surfaces after Chemical Pretreatments", 12 Natl. SAMPE Conf., Seattle, WA, Oct., 1980.

12. J. P. Wightman, W. Chen and B. Beck, "The Application of ESCA to Metal/Polymer Adhesion", 19th Eastern Analytical Symp., New York, NY, Nov., 1980.

13. J. P. Wightman and B. Beck, "Characterization of Ti 6(Al) - 4(V) Failure Surfaces by ESCA and SEM", 4th Ann. Meeting Adh. Soc., Savannah, GA, Feb., 1981.